Asymptotic behaviour of matrix elements between scar functions

2005 J. Phys. A: Math. Gen. 38 587

(http://iopscience.iop.org/0305-4470/38/3/005)

INSTITUTE OF PHYSICS PUBLISHING JOURNAL OF PHYSICS A: MATHEMATICAL AND GENERAL

J. Phys. A: Math. Gen. **38** (2005) 587–616 doi:10.1088/0305-4470/38/3/005

Asymptotic behaviour of matrix elements between scar functions

Eduardo G Vergini[1,2] **and David Schneider**[2]

[1] Departamento de Química C-IX, Universidad Autónoma de Madrid, Cantoblanco, 28049-Madrid, Spain
[2] Departamento de Física, Comisión Nacional de Energía Atómica. Av. del Libertador 8250, 1429 Buenos Aires, Argentina

Received 23 March 2004, in final form 16 November 2004
Published 23 December 2004
Online at stacks.iop.org/JPhysA/38/587

Abstract
Within the framework of the short periodic orbit theory in quantum chaos, matrix elements between scar functions play a central role. In this paper, we study the asymptotic behaviour of these matrix elements. In particular, we provide expressions for the overlap between scar functions and for matrix elements of the Hamiltonian. It is a remarkable fact that these matrix elements essentially depend on heteroclinic areas related to pairs of periodic orbits.

PACS numbers: 05.45.Mt, 03.65.Sq

1. Introduction

When a classical Hamiltonian system is chaotic, Gutzwiller's trace formula [1] provides a tool for the semiclassical evaluation of the energy spectrum in terms of the periodic orbits (POs) of the system. This periodic orbit theory has made considerable progress in last 15 years; for instance, resummation techniques have been applied to improve convergence properties [2, 3]. However, the theory suffers from a very serious limitation: the number of required POs increases exponentially with the Heisenberg time.

Recently, we have derived a semiclassical theory of short POs [4, 5]. This formalism allows us to obtain all the quantum information of a chaotic Hamiltonian system in terms of a very small number of short POs (which increases at most linearly with the Heisenberg time). The main idea of this approach is to replace the use of long POs by the evaluation of the interaction between short POs. In order to clarify this idea, it is worth emphasizing that related to each short PO (in a given energy region), there is a wavefunction living on the stable and unstable manifolds before they reach the first homoclinic point. We refer to these wavefunctions as *scar functions*, and their semiclassical construction is extensively explained in [6] (see also [7]). Then, by interaction between short POs we mean Hamiltonian matrix elements between the corresponding scar functions.

In this paper, we are mainly interested into the asymptotic behaviour of these matrix elements; for instance, we will study the overlap between scar functions and matrix elements of the Hamiltonian. For this reason, we do not consider the most general pair of scar functions, but only the simplest ones that in any way capture the asymptotic properties of matrix elements[3]. In particular, we are interested in the classical invariants which are responsible for that asymptotic behaviour. Those invariants will be evidently not only the stability index or the Maslov index which are related to individual POs, but also classical invariants depending on pairs of POs.

A scar function is constructed with the pieces of stable and unstable manifolds in the vicinity of a given periodic orbit, while these manifolds go away from the central orbit. When observed on a Poincaré surface of section, these pieces of manifolds form a cross. So, the semiclassical analysis of matrix elements between scar functions is mainly related to classical invariants defined by a pair of crosses. At this point, it is worth mentioning that manifolds with the same stability do not intersect. Hence, we can think about a pair of parallel crosses; that is, the stable piece of one cross is parallel to the stable piece of the other, and the same idea is applied to the pieces of unstable manifolds. Therefore, the unique classical invariant defined by two crosses is the symplectic area enclosed by the four pieces of manifolds. In this paper, we refer to this area as the heteroclinic area associated with the pair of periodic orbits, and we will see that this area plays a central role in the determination of matrix elements.

Of course, matrix elements also depend on a direction transverse to the Poincaré surface of section. Nevertheless, as we show in appendix A, matrix elements are very insensitive to such a direction. Actually, this direction plays a role when the periodic orbits live on different energy shells, and the study of this situation, which does not introduce new concepts, is discussed in appendix C. For these reasons, in the central part of the paper we only analyse matrix elements on a Poincaré surface of section.

The paper is organized as follows. Section 2 is devoted to explain the semiclassical construction of a scar function in the vicinity of a hyperbolic fixed point and to study its properties in detail. In section 3 we analyse an integral representation which is, in some way, asymptotically equivalent to the scar state; with this, we are able to obtain its coordinate representation. The next section contains the analysis of matrix elements, where equations (56) and (63) are the central expressions for the surface of section contribution to matrix elements. The last section is devoted to conclusions. Moreover, in appendix B we explain the essential ideas for the scar function construction in Hamiltonian systems with two degrees of freedom, and its reduction to a Poincaré surface of section. Finally, appendix D shows a particular example in the baker's map to clarify several ideas developed in the paper.

2. Scar functions

In this section, we will construct the scar function on a suitable Poincaré surface of section. In the vicinity of the fixed point representing the periodic orbit on the surface of section, the motion of the classical objects used for the construction of the scar function is governed by a hyperbolic Hamiltonian; see appendix B for a detailed explanation. Then, we will evaluate the scar state of a fixed hyperbolic point, first in the harmonic-oscillator basis and then, in the coordinate representation in the vicinity of the fixed point. We were unable to directly obtain a practical expression for the coordinate representation far away from the fixed point. For this reason, in the next section we will study an integral representation which seems suitable for that purpose.

[3] There are two types of scar functions: even and odd. In this paper, we only analyse matrix elements between even scar functions.

The classical Hamiltonian $H(q, p) = \lambda qp$ defines a hyperbolic point at the origin with Lyapunov exponent λ, where the unstable manifold lives on the q-axis and the stable one on the p-axis. For instance, the evolution of a point (q_0, p_0) with non-null energy occurs on the hyperbola branch $(q_0\,\mathrm{e}^{\lambda t}, p_0\,\mathrm{e}^{-\lambda t})$. We will assume that $H(q, p)$ describes the actual motion in the region $|q| < Q$ and $|p| < P$ of phase space and we are interested into the construction, restricted to this region, of wavefunctions with minimum energy dispersion. For the sake of simplicity, in the following we measure the time in units of λ^{-1}, q in units of Q and p in units of P. Then, the classical motion is described by

$$H(q, p) = qp, \tag{1}$$

in the region $|q| < 1$ and $|p| < 1$.

In terms of the usual creation–annihilation operators [8] $a^\dagger = (\hat{q} - \mathrm{i}\hat{p})/\sqrt{2\hbar}$ and $a = (\hat{q} + \mathrm{i}\hat{p})/\sqrt{2\hbar}$, the quantum Hamiltonian is

$$\hat{H} = \frac{\hat{p}\hat{q} + \hat{q}\hat{p}}{2} = \frac{\mathrm{i}\hbar}{2}(a^{\dagger 2} - a^2). \tag{2}$$

Moreover, the set of harmonic-oscillator states

$$|n\rangle = \frac{a^{\dagger n}|0\rangle}{\sqrt{n!}}, \qquad \text{for} \quad n = 0, \ldots, N_0, \tag{3}$$

is a convenient orthonormal basis for the description of wavefunctions restricted to the region $|q| < 1$ and $|p| < 1$ of phase space, if only excitations up to $N_0 \simeq 1/2\hbar$ are included[4]. In equation (3), the vacuum state in q-representation is given by $\langle q|0\rangle = (\pi\hbar)^{-1/4}\exp(-q^2/2\hbar)$.

In this section, we will restrict our calculation to scar states $|\phi\rangle$ with null mean energy because in the other case the calculation is cumbersome. However, in the next section we will show that they have minimum energy dispersion and consequently we will only be interested in scar states with such a restriction. Then, the problem of finding $|\phi\rangle$ that minimizes the energy dispersion σ, where by definition

$$\sigma^2 \equiv \frac{\langle\phi|\hat{H}^2|\phi\rangle}{\langle\phi|\phi\rangle}, \tag{4}$$

is equivalent to finding the least eigenvalue of $\hat{H}^2$ [6, 9]. Now, taking into account that $a^\dagger|n\rangle = \sqrt{n+1}|n+1\rangle$ and $a|n\rangle = \sqrt{n}|n-1\rangle$, it results in

$$\hat{H}^2|n\rangle = \frac{\hbar^2}{4}(-a_n|n+4\rangle + b_n|n\rangle - a_{n-4}|n-4\rangle), \tag{5}$$

with $a_n = \sqrt{(n+1)(n+2)(n+3)(n+4)}$ and $b_n = (n+1)(n+2) + (n-1)n$. It is clear from equation (5) that the matrix of $\hat{H}^2$ can be decomposed into four blocks, each one related to basis states four excitations away from each other. However, only two blocks provide solutions which are relevant in the semiclassical limit (the other two blocks play a role for the construction of scar functions with non-null mean energy). The first block is constructed with the subset of states $\{|0\rangle, |4\rangle, |8\rangle, \ldots\}$, and the second one with the subset $\{|1\rangle, |5\rangle, |9\rangle, \ldots\}$. The solution obtained from the first block is the so-called even scar function [6], and we will obtain its expansion coefficients

$$|\phi\rangle = \sum_{j=0}^{N} c_j|4j\rangle, \tag{6}$$

[4] The states given in equation (3) are eigenstates of $\hat{H}_0 = (\hat{p}^2 + \hat{q}^2)/2$, with eigenenergies $\hbar(n + 1/2)$. On the other hand, the borders of the admitted region along the manifolds have energy $H_0 = 1/2$ (for instance, $H_0\ (q = 1, p = 0) = H_0\ (q = 0, p = 1) = 1/2$). Then, the maximum excitation is restricted by the condition $\hbar(N_0 + 1/2) \leqslant 1/2$.

where $N = N_0/4 \simeq 1/8\hbar$. In this section, we take the limit $N \to \infty$ in order to consider the semiclassical limit $\hbar \to 0$.

By replacing (6) in (4) and using (5), we obtain

$$\Gamma^2 \equiv \frac{\sigma^2}{(\hbar^2/4)} = \frac{A}{B}, \tag{7}$$

where Γ is the so-called universal dispersion [6], with

$$A = \sum_{j=0}^{N} [c_j \sqrt{(4j+1)(4j+2)} - c_{j+1}\sqrt{(4j+3)(4j+4)}]^2, \tag{8}$$

and

$$B = \sum_{j=0}^{N} c_j^2. \tag{9}$$

As we mentioned previously, the coefficients c_j that minimize Γ^2 can be obtained from the eigenvalue problem $\hat{H}^2|\phi\rangle = \sigma^2|\phi\rangle$, where σ^2 is the least eigenvalue; that is, from equation (5) there results

$$-A_j c_{j+1} + B_j c_j - A_{j-1} c_{j-1} = \Gamma^2 c_j \tag{10}$$

for $j = 0, \ldots, N$, with

$$A_j = a_{4j} \qquad \text{and} \qquad B_j = b_{4j}. \tag{11}$$

This set of equations can be solved recursively (see [6]). On the other hand, to obtain an explicit asymptotic expression for Γ and the coefficients[5], we define a continuous function $c(z)$ in the range $0 < z \leqslant 1$, so that

$$c\left(\frac{j}{N+1}\right) = c_j$$

for $j = 1, \ldots, N$. Then, the recursive relation (10) transforms into the following ordinary differential equation,

$$4z^2 \frac{\mathrm{d}^2 c(z)}{\mathrm{d}z^2} + 8z \frac{\mathrm{d}c(z)}{\mathrm{d}z} + \left(1 + \frac{\Gamma^2}{4}\right) c(z) = 0 \tag{12}$$

restricted by the boundary condition $c(1) = 0$ (because $c_{N+1} = 0$). To obtain equation (12), we have expanded the roots in the coefficients A_j by assuming $j \gg 1$, so the differential equation is a poor approximation to the recursive relation for $z = O(1/N)$.

A positive well-behaved solution of equation (12) is

$$c(z) = -\frac{\sin[(\Gamma/4)\ln z]}{\sqrt{z(N+1)}}. \tag{13}$$

By considering that this expression is a good approximation to the coefficients for $j = 1, \ldots, N$, and taking $c_0 = \sqrt{6}c_1/(1 - \Gamma^2/2)$ from equation (10), we can evaluate the sums in equations (8) and (9) in terms of integrals for $j \geqslant 1$. Moreover, defining $u \equiv -(\Gamma/4)\ln z$, integrals are solved explicitly as follows (we are assuming that Γ is a small parameter that tends to zero when $N \to \infty$)

$$A = 4\Gamma \int_0^{u_1} \cos^2 u \, \mathrm{d}u + O(\Gamma^2) \simeq 2\Gamma \left(u_1 + \frac{\sin(2u_1)}{2}\right) \tag{14}$$

[5] These coefficients differ by $(-1)^j$ from the corresponding ones obtained in [6]. This fact is related to the selected phase in the definition of the creation–annihilation operators.

and

$$B = \frac{4}{\Gamma}\int_0^{u_1} \sin^2 u \, \mathrm{d}u + O(1) \simeq \frac{2}{\Gamma}\left(u_1 - \frac{\sin(2u_1)}{2}\right) \tag{15}$$

where $u_1 \equiv (\Gamma/4)\ln(N+1)$. The term $j = 0$ in equation (8) is not included in (14) because its order is equal to the order of the remainder (and the same argument is applicable to (15)). In the calculation of [6], we have retained these terms in order to obtain an interpolation formula for Γ, but here we are mainly interested in its asymptotic behaviour.

By assuming that $u_1 > 0$, we can replace equations (14) and (15) in (7) arriving at the conclusion that $\sin(2u_1) \simeq 0$, or equivalently that u_1 converges to $\pi/2$. Then, using that $u_1 \equiv (\Gamma/4)\ln(N+1)$, $N \simeq 1/8\hbar$ and $\sigma \equiv \hbar\Gamma/2$ (see (7)), we obtain

$$\sigma = \frac{\pi\hbar}{|\ln\hbar|}[1 + O(|\ln\hbar|^{-1})]. \tag{16}$$

To improve c_j for fixed values of j as $N \to \infty$, we note first of all that $A = O(\Gamma) = O(1/\ln N)$. This means that each term on the right-hand side of equation (8) tends to zero in the limit $N \to \infty$. Then, assuming that c_j converges to the non-null finite value $\tilde{c}_j$ in this limit, there results

$$\frac{\tilde{c}_j}{\tilde{c}_{j+1}} = \sqrt{\frac{(4j+3)(4j+4)}{(4j+1)(4j+2)}}. \tag{17}$$

Hence, a solution of (17) which moreover converges asymptotically (for $j \gg 1$) to $1/\sqrt{j} = \lim_{N\to\infty} c(j/N)$, is given by

$$\tilde{c}_j = \frac{(2\pi)^{1/4}\sqrt{(4j)!}\,\tilde{\Gamma}(j+1/2)}{2^{2j}(2j)!\,\tilde{\Gamma}(j+3/4)} \tag{18}$$

where $\tilde{\Gamma}(x)$ is the gamma function of x.

Finally, by coupling equations (13) (which works for j/N a fixed value) and (18) (which works for j a fixed value), and using the normalization provided by equation (15) ($B \to \pi/\Gamma$), we obtain the following normalized asymptotic expression[6] (exact in the limit $N \to \infty$) for $j = 0, \ldots, N$

$$c_j = \sqrt{\frac{\Gamma}{\pi}}\tilde{c}_j \sin\left[\frac{\Gamma}{4}\ln\left(\frac{N+2}{j+1}\right)\right]. \tag{19}$$

We stress that $\tilde{c}_j$ (see (18)) is well approximated by $\tilde{c}_j = [1 - \beta/j + O(j^{-2})]/\sqrt{j}$ for $j \geqslant 1$, when $\beta = 1/16$. This type of approximation was considered in [6], where β was obtained numerically as a function of N and an expression was provided in the range $1 \leqslant N \leqslant 10^5$. Nevertheless, according to the previous asymptotic analysis such expression does not work in the limit $N \to \infty$.

In order to obtain an equivalent expression for the coefficients of the odd scar function (which is expanded in terms of $\{|1\rangle, |5\rangle, |9\rangle, \ldots\}$), we simply substitute $4j$ for $4j+1$ in equations (6), (8), (11) and (17). Then, the solution is again given by equation (19) whether we use, in place of equation (18), the following expression,

$$\tilde{c}_j = \frac{(2\pi)^{1/4}\sqrt{(4j+1)!}\,\tilde{\Gamma}(j+3/4)}{2^{2j+1/2}j!\,\tilde{\Gamma}(2j+3/2)},$$

which is well approximated by $\tilde{c}_j = [1 - 3/16j + O(j^{-2})]/\sqrt{j}$ for $j \geqslant 1$.

[6] We have included a correction of the order N^{-1} inside the argument of ln(.) to provide an expression valid for all N. This expression works very well for all N whether a precise value for Γ is used; for instance, the value provided by equation (53) (or (54) for odd scar functions) of [6].

Recently, a new construction of hyperbolic structures was presented in [10]. In that work, the so-called leading scar state is given in the harmonic-oscillator basis by the coefficients $\tilde{c}_j$. It is worth mentioning that such simplification is not useful for our purposes. In fact, it is easy to see (from equations (8) and (9)) that by using simply the coefficients $\tilde{c}_j$ for $j = 0, \ldots, N$, there result[7] $A \sim N$ and $B \sim \ln N$ respectively; so, the universal dispersion Γ goes to infinity in place of going to zero in the limit $N \to \infty$.

In order to characterize the properties of the scar function note that even momenta of $\hat{H}$ satisfy (use the relation $\hat{H}^2|\phi\rangle = \sigma^2|\phi\rangle$)

$$\langle\phi|\hat{H}^{2n}|\phi\rangle = \sigma^{2n} = O(|\ln\hbar|^{-2n}) \tag{20}$$

where the leading order of σ is given by equation (16), while $\langle\phi|\hat{H}^{2n+1}|\phi\rangle = 0$. Therefore, a function that converges to the scar function has to satisfy the previous properties in the semiclassical limit.

We finish this section by obtaining in leading order, the scar function as an expansion in the vicinity of $q = 0$. We assume that the elimination of a finite number of terms in equation (6) does not change the leading order. Then, it is possible to use the following asymptotic expression (valid for $j \gg 1$) for harmonic-oscillator wavefunctions around $q = 0$

$$\langle q|4j\rangle \simeq \frac{1}{(2\pi^2 j\hbar)^{1/4}} \sum_{l=0}^{2j} (-1)^l \frac{(2j)!}{(2l)!(2j-l)!} \left(\frac{4q^2}{\hbar}\right)^l. \tag{21}$$

Replacing equations (19) and (21) in (6) and changing the order of the sums there results

$$\phi(q) \simeq \frac{\Gamma^{1/2}}{\pi(2\hbar)^{1/4}} \sum_{l=0} \frac{(-1)^l}{(2l)!} \left(\frac{4q^2}{\hbar}\right)^l \sum_{j(\gg l)}^{N} (2j)^l j^{-3/4} \sin[(\Gamma/4)\ln(N/j)].$$

We dropped out many terms of the sum over j in order to satisfy $j \gg l$, and the approximation $(2j)!/(2j-l)! \simeq (2j)^l$ was used. Then, the sum over j is evaluated with an integration over the variable $u \equiv -(\Gamma/4)\ln z$ as before in equations (14) and (15); it gives $\sum_j \simeq 2^l N^{l+1/4} 4\Gamma/(4l+1)^2$. Finally, the leading order of the expansion around $q = 0$ results (recall that $N \simeq 1/8\hbar$ and $\Gamma \simeq 2\pi/|\ln\hbar|$)

$$\phi(q) \simeq \frac{2^{5/2}\pi^{1/2}}{|\ln\hbar|^{3/2}\hbar^{1/2}} \sum_{l=0} \frac{(-1)^l}{(2l)!(4l+1)^2} \left(\frac{q}{\hbar}\right)^{2l}. \tag{22}$$

From the last equation we observe that individual terms do not contribute to $\phi(q)$ near $q = 0$ because they are of order $\hbar^{-1/4}$; for instance, $\langle q|0\rangle = (\pi\hbar)^{-1/4}\exp(-q^2/2\hbar)$. Equation (22) corresponds to even scar functions, and it only provides a practical expression in the range $|q| < O(\hbar)$. For odd scar functions we simply multiply (22) by $\mathrm{sgn}(q)$. Finally, the action of $\hat{H}$ on ϕ is obtained from equation (22), by applying $\hat{H} = -\mathrm{i}\hbar(1/2 + q\,\mathrm{d}/\mathrm{d}q)$. There results

$$\hat{H}\phi(q) \simeq \frac{-\mathrm{i}\hbar^{1/2}2^{3/2}\pi^{1/2}}{|\ln\hbar|^{3/2}} \sum_{l=0} \frac{(-1)^l}{(2l)!(4l+1)} \left(\frac{q}{\hbar}\right)^{2l}. \tag{23}$$

3. An integral representation

The objective of this section is to find an integral representation of the scar state. We will show that this representation proves very suitable in order to obtain the q-representation in the intermediate region $q \sim \sqrt{\hbar}$.

[7] By using c_j, $A \sim 1/\ln N$.

Based on several previous works [11], we propose the following integral representation[8]

$$|\tilde{\phi}\rangle = \int_{-T/2}^{T/2} \mathrm{d}t\ f(2t/T)\,\mathrm{e}^{\mathrm{i}\theta t}\hat{U}^t|0\rangle, \tag{24}$$

where $T \equiv |\ln\hbar|$ is of the order of the so-called Ehrenfest time, and θ is a parameter (we will omit the explicit dependence of different quantities on θ). The real function $f(x)$ is defined in the range $|x| \leqslant 1$, and we will search for the smooth function $f(x)$ that minimizes the energy dispersion of $|\tilde{\phi}\rangle$. For this purpose, we first of all evaluate the autocorrelation function $F(t) \equiv \langle\tilde{\phi}|\hat{U}^t\,\mathrm{e}^{\mathrm{i}\theta t}|\tilde{\phi}\rangle$ for infinitesimal times ($t \sim 0$),

$$F(t) = \int_{-T/2}^{T/2}\int_{-T/2}^{T/2} \mathrm{d}t_1\,\mathrm{d}t_2 f\left(\frac{2t_1}{T}\right) f\left(\frac{2t_2}{T}\right)\mathrm{e}^{\mathrm{i}\theta(t+t_1-t_2)}\langle 0|\hat{U}^{t+t_1-t_2}|0\rangle. \tag{25}$$

By changing to new variables $s \equiv (t_1+t_2)/T$ and $x \equiv (t_1-t_2)/T$, and using the well-known result[9] $\langle 0|\hat{U}^{t+t_1-t_2}|0\rangle = 1/\sqrt{\cosh(t+t_1-t_2)}$, equation (25) results in

$$F(t) = \frac{T^2}{2}\int_{-1}^{1} \mathrm{d}x\, h(x)\frac{\mathrm{e}^{\mathrm{i}\theta(t+xT)}}{\sqrt{\cosh(t+xT)}}, \tag{26}$$

with

$$h(x) = \int_{-(1-|x|)}^{1-|x|} \mathrm{d}s\ f(s+x)f(s-x). \tag{27}$$

Assuming $h(x)$ bounded, the range of x contributing to the integral in equation (26) is $O(1/T)$ (because $t \sim 0$). Then, by using the following expansion $f(s+x)f(s-x) = f(s)^2 + x^2[f''(s)f(s) - f'(s)^2] + O(T^{-3})$, we obtain after an elementary calculation

$$h(x) = \alpha - \beta|x| - 2\gamma x^2 + O(T^{-3}), \tag{28}$$

with $\alpha = \int_{-1}^{1} f(s)^2\,\mathrm{d}s$, $\beta = f(-1)^2 + f(1)^2$ and $\gamma = \int_{-1}^{1} f'(s)^2\,\mathrm{d}s - [f(1)f'(1) - f(-1)f'(-1)]$.

On the other hand, using the change of variable $y \equiv t + xT$ in equation (26), there results[10]

$$F(t) = \frac{T}{2}\int_{-\infty}^{\infty} \mathrm{d}y\, h\left(\frac{y-t}{T}\right)\frac{\mathrm{e}^{\mathrm{i}\theta y}}{\sqrt{\cosh y}} + O(\mathrm{e}^{-T/2}). \tag{29}$$

Hence, taking into account that by definition $F(t) = \sum_{n=0}(-\mathrm{i})^n M_n t^n/n!$ where

$$M_n \equiv \langle\tilde{\phi}|(\hat{H}/\hbar - \theta)^n|\tilde{\phi}\rangle,$$

we obtain after n times differentiation of equation (29)

$$M_n = \frac{(-\mathrm{i})^n T^{1-n}}{2}\int_{-\infty}^{\infty} \mathrm{d}y\, h^{(n)}\left(\frac{y}{T}\right)\frac{\mathrm{e}^{\mathrm{i}\theta y}}{\sqrt{\cosh y}} + O(\mathrm{e}^{-T/2}). \tag{30}$$

Using (28) and (30), the variance of $|\tilde{\phi}\rangle$ results[11] in

$$\frac{\sigma^2}{\hbar^2} \equiv \frac{M_2}{M_0} - \left(\frac{M_1}{M_0}\right)^2 = \frac{\beta}{\alpha I_0 T} + \frac{4\gamma}{\alpha T^2} + \frac{\beta^2}{T^2}O(1) + O(T^{-3}), \tag{31}$$

[8] The variable t in equation (24) is an adimensional quantity. According to the previous section, it is the time in units of λ^{-1}.

[9] $\langle 0|\hat{U}^t|0\rangle = \int\langle 0|q\rangle\langle q|\hat{U}^t|0\rangle\,\mathrm{d}q = 1/\sqrt{\cosh t}$ results from $\langle q|\hat{U}^t|0\rangle = (\pi\hbar)^{-1/4}\exp[-(q^2/2\hbar)\,\mathrm{e}^{-2t} - t/2]$. The used expression for $\langle q|\hat{U}^t|0\rangle$ is exact because the Hamiltonian is quadratic; its accuracy is simply verified by noting that it satisfies the Schrödinger equation, $\mathrm{i}\hbar\partial_t = -\mathrm{i}\hbar(1/2 + q\,\partial_q)$.

[10] By making the limits of integration $\pm\infty$, we introduce an error of the order $\mathrm{e}^{-T/2}$.

[11] In order to reduce the calculation, note that $h(x)$ is an even function and so, its derivatives $h^{(n)}(x)$ have defined parity. For instance, using (36) we have $h^{(1)}(x) \simeq 1 - \pi^2 x + \pi^2 x^2[\mathrm{sgn}(x) + 2x\delta(x)/3]$.

where I_0 is the $n = 0$ case of the following definition:

$$I_n \equiv \int_0^\infty \mathrm{d}y\, y^n \frac{\cos(\theta y)}{\sqrt{\cosh(y)}}. \tag{32}$$

It is clear from (31) that in order to minimize the variance as $T \to \infty$, β must be equal to zero. This condition means that $f(1) = f(-1) = 0$ (see (28)) and consequently γ reduces to $\gamma = \int_{-1}^{1} f'(x)^2\,\mathrm{d}x$.

In what follows, we will find the function $f(x)$ that minimizes the leading order of σ^2, or equivalently (see (31)) that minimizes the functional

$$\Phi(f) \equiv \frac{\gamma}{\alpha} = \frac{\int_{-1}^{1} f'(x)^2\,\mathrm{d}x}{\int_{-1}^{1} f(x)^2\,\mathrm{d}x}. \tag{33}$$

In first place, note that $f(x)$ must satisfy

$$\frac{\int_{-1}^{0} f'(x)^2\,\mathrm{d}x}{\int_{-1}^{0} f(x)^2\,\mathrm{d}x} = \frac{\int_{0}^{1} f'(x)^2\,\mathrm{d}x}{\int_{0}^{1} f(x)^2\,\mathrm{d}x} \tag{34}$$

because if the right-hand side of equation (34) is, for instance, smaller than the left side, it is easy to show that $\Phi(f) > \Phi(\tilde{f})$, where $\tilde{f}(x) = f(x)$ for $x \geqslant 0$, and $\tilde{f}(x) = f(-x)$ for $x < 0$. Therefore, from equation (34) it results $\Phi(f) = \Phi(\tilde{f})$, and evidently we can reduce the search to even functions. Then, we expand $f(x)$ in terms of orthonormal even functions (vanishing at $x = 1$) in the range $|x| \leqslant 1$, as follows:

$$f(x) = \sum_{n=0} a_n \cos[\pi x(n + 1/2)].$$

By replacing this expansion in equation (33), $\Phi(f)$ transforms into the ratio of two quadratic forms

$$\Phi(f) = \frac{\sum_{n=0} a_n^2 \pi^2 (n + 1/2)^2}{\sum_{n=0} a_n^2}.$$

The minimum value of this ratio is equal to the least eigenvalue [9] of the diagonal matrix with elements $\pi^2(n + 1/2)^2$ (for $n = 0, 1, \ldots$) on the diagonal, which corresponds to $n = 0$. In conclusion, the function

$$f(x) = \cos(\pi x/2) \tag{35}$$

minimizes γ/α and the minimum value results $\pi^2/4$. Hence, from equation (31) the leading order of the energy dispersion is $\sigma/\hbar = \pi/T$, and this value is equal to that obtained in the previous section for the scar function (see (16)). It is interesting to see that this asymptotic value is independent of the parameter θ, which is up to order T^{-1} the mean energy of $|\tilde{\phi}\rangle$ divided by $\hbar$.

To study similarities and differences among hyperbolic structures with different mean energies and between the scar function and the proposed integral representation, we evaluate the next order of σ and the 4-momentum M_4/M_0. To do this, we first substitute (35) in (27) and obtain

$$h(x) = (1 - |x|)\cos(\pi x) + \frac{1}{\pi}\sin(\pi|x|) = 1 - \frac{\pi^2}{2}x^2 + \frac{\pi^2}{3}|x|^3 + O(x^4). \tag{36}$$

By substituting (36) in (30), the energy dispersion up to order T^{-2} results in

$$\frac{\sigma}{\hbar} = \frac{\pi}{T + I_1/I_0} + O(T^{-3}), \tag{37}$$

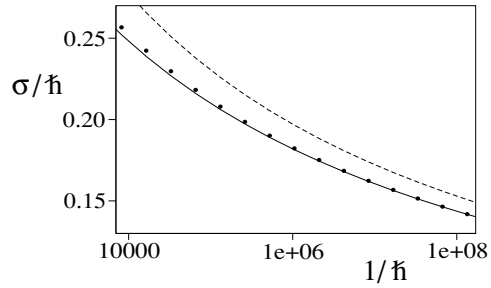

Figure 1. Plot of $\sigma/\hbar$ as a function of $1/\hbar$, for the scar function $\phi(q)$ (●), the numerical approximation $\pi/(|\ln\hbar|+3.45)$ (——); and the obtained analytical expression (37) for the integral representation $\tilde{\phi}(q)$ (- - - -).

where a numerical evaluation near $\theta = 0$ gives $I_1/I_0 \simeq 2.12 - 16.75\theta^2$. It is evident from (37) that for a fixed value of T, the minimum dispersion is obtained for $\theta = 0$; that is, when the mean energy is zero.

On the other hand, we mention that although equation (37) provides a good tool to compare the dispersion of hyperbolic structures with different mean energies, the dispersion of the scar function (section 2) is smaller (to order T^{-2}) than the value obtained in (37); a numerical estimation gives $\sigma < \pi\hbar/(T + 3.45)$ for the even scar function[12]. For instance, in figure 1 we compare the dispersion of the scar function (see [6] for a numerical computation) with the corresponding integral representation, as obtained from (37) for $\theta = 0$. This suggests that the proposed integral representation does not converge exactly to the scar function in the semiclassical limit. To probe this assertion, we observe that the 4-momentum of the integral representation results $M_4/M_0 = 4\pi^2/I_0T^3 + O(T^{-4})$, while for the scar function it is $O(T^{-4})$ (see (20)).

Now, we evaluate the q-representation of $|\tilde{\phi}\rangle$. First around $q = 0$, which gives a practical solution for $|q| < O(\hbar)$, then for $q \sim \sqrt{\hbar}$, and finally for $q \sim 1$; in the following we only analyse the case $\theta = 0$. Substituting (35) in (24) and normalizing $|\tilde{\phi}\rangle$ with the help of (30) ($M_0 = I_0T + O(T^{-1})$, where $I_0 = \tilde{\Gamma}(1/4)^2/(8\pi)^{1/2}$ for $\theta = 0$) we obtain

$$\tilde{\phi}(q) = M_0^{-1/2} \int_{-T/2}^{T/2} \mathrm{d}t\ \cos(\pi t/T) \frac{1}{(\pi\hbar)^{1/4}} \exp[-(q^2/2\hbar)\,\mathrm{e}^{-2t} - t/2]. \quad (38)$$

It is evident from this equation that $\tilde{\phi}(q)$ is an even function, so in the following we only analyse the $q \geqslant 0$ case. After expanding the exponential around $q = 0$, the contribution of each term to the time integral is reduced to the vicinity of $t \simeq -T/2$. Then, the leading order of $\tilde{\phi}(q)$ is

$$\tilde{\phi}(q) \simeq \frac{2^{11/4}\pi}{\tilde{\Gamma}(1/4)T^{3/2}\hbar^{1/2}} \sum_{l=0} \frac{(-1)^l}{2^l l!(4l+1)^2} \left(\frac{q}{\hbar}\right)^{2l}. \quad (39)$$

There are some similarities between the previous equation and the expansion of $\phi(q)$ around $q = 0$ (see (22)). Observe that the two expansions have the same $T = |\ln\hbar|$ behaviour, and the same dependence on q up to second order; namely, $1 - q^2/50\hbar^2$.

[12] We were unable to obtain analytically the dispersion of the scar function up to order T^{-2}. However, the interpolation formula derived in [6] provides the asymptotic value $\pi\hbar/(T + 3.62)$. Then, from the previous value and the numerical calculation of figure 1, the expression $\sigma \simeq \pi\hbar/(T + \alpha)$, where $3.45 < \alpha \simeq 3.62$, seems to be a good estimation.

In the intermediate region $q \sim \sqrt{\hbar}$, the change of variable $y \equiv 2[t - t_0(q)]$ transforms equation (38) into

$$\tilde{\phi}(q) = \frac{M_0^{-1/2}}{(2\pi)^{1/4}\sqrt{q}} \int_{-T-2t_0}^{T-2t_0} \cos\left[\frac{\pi}{2T}(y + 2t_0)\right] \exp[-(\mathrm{e}^{-y} + y)/4] \frac{\mathrm{d}y}{2}, \quad (40)$$

where

$$t_0(q) \equiv \tfrac{1}{2}\ln(2q^2/\hbar). \quad (41)$$

This integral can be solved in a vicinity of $t_0(q) = 0$ by making the limits of integration $\pm\infty$; see appendix E. Then, in the range $\hbar\sqrt{2\ln T} < q < O(T^{-2})$, the following expression results,

$$\tilde{\phi}(q) = \frac{\cos(\pi t_0/T) - \alpha\pi \sin(\pi t_0/T)/T + O(T^{-2})}{\sqrt{qT}} \quad (42)$$

where

$$\alpha \equiv \frac{\int_{-\infty}^{\infty} y \exp[-(\mathrm{e}^{-y} + y)/4]\,\mathrm{d}y}{\int_{-\infty}^{\infty} 2\exp[-(\mathrm{e}^{-y} + y)/4]\,\mathrm{d}y} \simeq 1.4206.$$

For $t_0 < -T/2$, $\tilde{\phi}(q)$ is approximately constant, as it can be derived from equation (39). On the other hand, it is not difficult to observe that $\tilde{\phi}(q)$ decays exponentially for $t_0 > T/2$. After the change of variable $x \equiv y + \ln(2q^2)$, equation (40) becomes

$$\tilde{\phi}(q) = \frac{\pi + O(T^{-2})}{2^{5/4}\tilde{\Gamma}(1/4)T^{3/2}} \int_0^{\infty} x \exp[(-2q^2\,\mathrm{e}^{-x} + x)/4]\,\mathrm{d}x,$$

and this expression can be estimated, for $q \sim 1$, by

$$\tilde{\phi}(q) \sim 0.42T^{-3/2}(1 + 3/q)\,\mathrm{e}^{-2q-0.3q^2}.$$

The next question is to know to what extent $\tilde{\phi}(q)$ is a good approximation for the scar function $\phi(q)$. In fact, we have verified from equations (22) and (39) that they differ in the vicinity of $q = 0$. However, we stress that $\phi(q)$ and $\tilde{\phi}(q)$ are the same in leading order around $q = \sqrt{\hbar}$. To see this, we note that only the region $c\hbar < q < c'$, with c and c' arbitrary positive constants, is relevant for the evaluation of some diagonal matrix elements in leading order. For instance, by using the leading order of $\tilde{\phi}(q)$ from equation (42) and the change of variables $x \equiv 2t_0(q)/T$, there results

$$2\int_{c\hbar}^{c'} \tilde{\phi}(q)^2\,\mathrm{d}q \simeq \int_{-1}^{1} \cos(\pi x/2)^2\,\mathrm{d}x = 1.$$

This means that the contribution of the regions $|q| < c\hbar$ and $|q| > c'$ to $\langle\tilde{\phi}|\tilde{\phi}\rangle$ is of the order T^{-1}.

As another example, we consider the mean value of $\hat{H}^2$. By using that $\hat{H} = -\mathrm{i}\hbar(1/2 + q\,\mathrm{d}/\mathrm{d}q)$, we obtain from equation (42)

$$\hat{H}\tilde{\phi}(q) \simeq \frac{\mathrm{i}\hbar\pi}{T^{3/2}} \frac{\sin[\pi t_0(q)/T] + (\alpha\pi/T)\cos[\pi t_0(q)/T]}{\sqrt{q}}. \quad (43)$$

Then, using the leading order of equation (43) and working as before, there results

$$2\int_{c\hbar}^{c'} |\hat{H}\tilde{\phi}(q)|^2\,\mathrm{d}q \simeq (\pi\hbar/T)^2 \int_{-1}^{1} \sin(\pi x/2)^2\,\mathrm{d}x = (\pi\hbar/T)^2,$$

which gives the right value for $\langle\tilde{\phi}|\hat{H}^2|\tilde{\phi}\rangle$ in leading order. Hence, taking into account that the previous diagonal matrix elements are the same for $|\tilde{\phi}\rangle$ and $|\phi\rangle$ in leading order, $\tilde{\phi}(q)$ and $\phi(q)$ must coincide, in leading order, in the intermediate region $q \sim \sqrt{\hbar}$. So, in this region

$$\phi(q) \simeq \tilde{\phi}(q) \simeq \frac{\cos[\pi t_0(q)/T]}{\sqrt{qT}}, \quad (44)$$

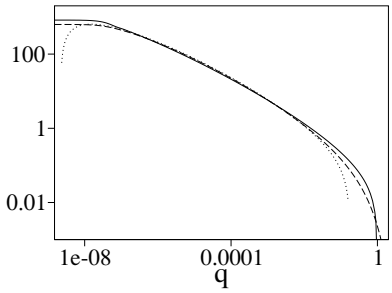

Figure 2. For $1/8\hbar = 10^7$, we compare $\phi(q)$ (——), $\tilde{\phi}(q)$ (- - - -) and the estimation given by equation (42) ($\cdots\cdots$). The three functions are the same to leading order in the intermediate region $q \sim \sqrt{\hbar}$.

and

$$\hat{H}\phi(q) \simeq \hat{H}\tilde{\phi}(q) \simeq \frac{\mathrm{i}\hbar\pi}{T^{3/2}} \frac{\sin[\pi t_0(q)/T]}{\sqrt{q}}. \tag{45}$$

We mention that equations (44) and (45) are also satisfied, in leading order, by other hyperbolic structures with null mean energy and minimum dispersion. For instance, the integral construction

$$\int_{-T_m/2}^{T_m/2} \cos(\pi t/T_m)\hat{U}^t|4m\rangle \,\mathrm{d}t, \qquad \text{for} \quad m = 0, 1, \ldots, \tag{46}$$

where $T_m \equiv T - \ln(8m+1)$, satisfies the previous properties[13] and corresponds to hyperbolic structures living in the region $|q| < 1$ and $|p| < 1$. In this respect, it is interesting to mention that the scar function $\phi(q)$ can be represented, in terms of the previous defined structures, over the entire q range. Unfortunately, it is difficult to obtain an explicit expression for $|\phi\rangle$ in terms of the set provided in equation (46). In any case, it is not difficult to see that the most important contribution is given by the $m = 0$ term, because it has the smallest dispersion.

In figure 2 we compare $\phi(q)$, $\tilde{\phi}(q)$ and the analytical approximation to $\tilde{\phi}(q)$ in the intermediate region $q \sim \sqrt{\hbar}$ (see equation (42)). As was established in equation (44), the three functions are the same (to leading order) in this region.

4. Matrix elements between scar functions

We will study a Poincaré surface of section matrix elements between scar functions for a two degrees of freedom Hamiltonian system. The contribution provided by a transverse direction to the surface of section is discussed in appendices A and C. We assume that on a given Poincaré surface of section with coordinates (q, p), there are two fixed points with the same stability index (some times called the Lyapunov exponent) λ at $(0, 0)$ and (q_0, p_0), respectively[14]. Moreover, their stable manifolds are parallels to the p-axis for a range P around the fixed points; in the same way, the unstable manifolds are parallels to the q-axis for a range Q (see figure 3). We show in appendix A that the previous picture is generic.

In terms of the units used in section 2 for time, length and momentum, the short time dynamics in the vicinity of the fixed point $(0, 0)$ is fully described by the local Hamiltonian $H(q, p) = qp$ for $|q|, |p| < 1$. Moreover, the Hamiltonian $H'(q, p) = (q - q_0)(p - p_0)$

[13] The $m = 0$ case corresponds to the integral representation of equation (38).
[14] This restriction is relaxed in appendix C.

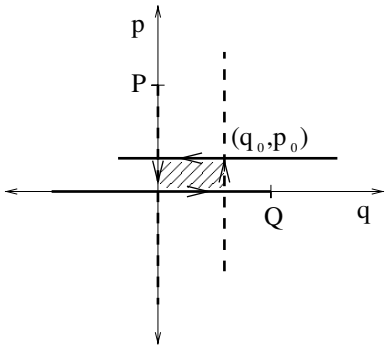

Figure 3. Plot of the two fixed points at (0, 0) and (q_0, p_0) considered in the calculation of matrix elements, and their stable (- - - -) and unstable (——) manifolds over a finite range. Shaded with oblique lines, the absolute value $A = q_0 p_0$ of the heteroclinic area defined by the manifolds is depicted. Arrows indicate the direction of the flux on the manifolds.

for $|q - q_0|, |p - p_0| < 1$ describes the dynamics in the vicinity of the other fixed point. In this respect, we would like to emphasize that these Hamiltonians are not just the restriction to the surface of section of the full Hamiltonian. They contain global information about the motion along the corresponding periodic orbit. In fact, they provide a continuous version of the motion described by the return map in the vicinity of each fixed point. This point is discussed in detail in appendix B.

Let $\phi(q)$ be the scar function centred at $(0, 0)$ as was defined in previous sections; this wavefunction is the restriction to the Poincaré surface of section of the scar function constructed in [6]. Then, the scar function $\phi'(q)$ centred at (q_0, p_0) is simply a translation of $\phi(q)$, obtained by the application of a Heisenberg operator [12]

$$\phi'(q) = \phi(q - q_0)\, \mathrm{e}^{\mathrm{i}p_0(q-q_0/2)/\hbar}. \tag{47}$$

Actually, there is an ambiguous phase in the definition of $\phi'(q)$, and we have selected the one that provides real matrix elements; in the following, primed wavefunctions indicate translations like that in equation (47). Furthermore, the action of $\hat{H}'$ on $\phi'(q)$ is equivalent to the translation of $\hat{H}\phi(q)$,

$$\hat{H}'\phi'(q) = [\hat{H}\phi](q - q_0)\, \mathrm{e}^{\mathrm{i}p_0(q-q_0/2)/\hbar}. \tag{48}$$

We emphasize that the two scar functions have the same mean energy, but this point deserves an explanation. The energy considered in the previous sections is related to the transverse motion, and we have taken this energy equal to zero for the two scar functions. However, a scar function also includes the energy of the motion along the orbit (see [6] and also appendix B); this energy takes discrete values according to a rule of the Bohr–Sommerfeld type. Then, we assume that the two scar functions also have the same energy along the corresponding orbit (the same Bohr–Sommerfeld energy). The effect of different mean energies (when the periodic orbits live on different energy shells) on matrix elements is discussed in appendix C.

By taking into account that $\phi(q)$ is a real even function, $\phi(q)\phi(q - q_0)$ is even around $q = q_0/2$. Then, the overlap between scar functions is

$$\langle\phi|\phi'\rangle = 2\int_{q_0/2}^{\infty} \mathrm{d}q\, \phi(q)\phi(q - q_0) \cos[p_0(q - q_0/2)/\hbar]. \tag{49}$$

So, in order to obtain a first estimate of the overlap, we consider the function $\phi_0(q) = 1/\sqrt{|q|T}$, which satisfies $\phi_0(q) \geqslant \phi(q)$ for all q and $\phi_0(q) \simeq \phi(q)$ for $q \sim \sqrt{\hbar}$ (see equations (22) and (44)). Then, after the change of variable $x \equiv 2q/q_0 - 1$, the overlap becomes

$$\langle \phi_0 | \phi_0' \rangle = \frac{2}{T} \int_0^\infty \frac{\cos(\alpha x)\, \mathrm{d}x}{\sqrt{|1-x^2|}} = \frac{\pi}{T}[J_0(\alpha) - Y_0(\alpha)] \tag{50}$$

where J_0 and Y_0 are the Bessel and Neumann functions of zero order, respectively. $\alpha \equiv A/2\hbar$, and $A = q_0 p_0$ is the absolute value of the heteroclinic area enclosed by the four manifolds (see figure 3). The heteroclinic area is the symplectic area defined by the line integral $\oint p\, \mathrm{d}q$ along the rectangle delimited by the four manifolds, where the path is taken following the direction of the flux on the manifolds. In this example, the direction is anticlockwise and consequently the heteroclinic area is negative.

For $A > \hbar$ (large values of α), equation (50) takes the form

$$\langle \phi_0 | \phi_0' \rangle \simeq \frac{2\sqrt{\pi}}{T} \frac{\cos(A/2\hbar)}{\sqrt{A/2\hbar}}. \tag{51}$$

It is interesting to note that equation (51) behaves like a quantization rule, where the overlap is zero for $A = 2\pi\hbar(n+1/2)$, with n an integer. For large values of α, it is instructive to estimate the integral in equation (50) by considering simply its contribution near the divergence at $x = 1$ (take $x + 1 \sim 2$ and the lower limit of integration equal to $-\infty$) as follows:

$$\frac{2}{T} \int_{-\infty}^{\infty} \mathrm{d}x\, \frac{\cos[\alpha(x-1)+\alpha]}{\sqrt{2|1-x|}} = \frac{2\sqrt{\pi}}{T} \frac{\cos(A/2\hbar)}{\sqrt{A/2\hbar}}. \tag{52}$$

This rough estimate gives the same result obtained in equation (51). We would also like to mention a heuristic approximation derived from the fact that manifolds intersect at the points $z_1 \equiv (0, p_0)$ and $z_2 \equiv (q_0, 0)$; see figure 3. Taking into account that the Husimi of scar functions (a phase space probability density) concentrates along the manifolds, we hope that the main contribution to the overlap comes from the vicinity of these intersecting points, the so-called heteroclinic points. Hence, the following estimate appears reasonable,

$$\langle \phi_0 | \phi_0' \rangle \sim \langle \phi_0 | z_1 \rangle \langle z_1 | \phi_0' \rangle + \langle \phi_0 | z_2 \rangle \langle z_2 | \phi_0' \rangle \tag{53}$$

where $|z_1\rangle$ and $|z_2\rangle$ are coherent states centred at the intersecting points. The first term of the rhs results $\exp(\mathrm{i}A/2\hbar)2(\pi\hbar/A)^{1/2}/T$, while the second one gives its complex conjugated[15]. Therefore, this simple estimate, being $\sqrt{2}$ times the one given by equation (51), provides the main behaviour of the overlap.

In the following, we consider a better approximation to the overlap. Evidently, the most important discrepancy between ϕ_0 and ϕ is that ϕ_0 diverges at $q = 0$ and decreases algebraically for large q, while ϕ is finite near zero and decreases exponentially around $q = 1$. Hence, the following correction to ϕ_0, which works in the neighbourhood of $q = 0$, is proposed,

$$\phi_1(q) = \frac{1}{\sqrt{q_1 T}} - \frac{1}{\sqrt{|q|T}} \qquad \text{for} \quad |q| \leqslant q_1$$

where $q_1 = T^2\hbar/2^5\pi$, and $\phi_1(q) = 0$ otherwise. With this definition, the function $\phi_0 + \phi_1$ behaves like ϕ near $q = 0$ (see (22)), and $\phi_0(q) + \phi_1(q) \geqslant \phi(q)$ for all q. Then, the correction $\langle \phi_1 | \phi_0' \rangle$ (to the overlap given in equation (51)) can be obtained simply for q_0 and $p_0 \sim \sqrt{\hbar}$, by making $\phi_0'(q) \sim \phi_0'(0)$

$$\langle \phi_1 | \phi_0' \rangle \sim \frac{2\cos(A/2\hbar)}{T\sqrt{q_0}} \int_{-q_1}^{q_1} \left(\frac{1}{\sqrt{q_1}} - \frac{1}{\sqrt{|q|}} \right) \mathrm{d}q = -\frac{T}{4\pi} \sqrt{p_0} \langle \phi_0 | \phi_0' \rangle, \tag{54}$$

[15] For the calculation of $\langle z_2 | \phi_0' \rangle$ and $\langle \phi_0 | z_1 \rangle$, it is easier to work in p-representation.

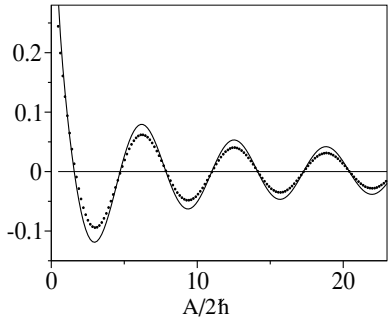

Figure 4. For $1/8\hbar = 10^5$, the plot compares, as a function of $A/2\hbar$, a numerical evaluation of the overlap between scar functions ($\cdots\cdots$) according to (49), with the estimate given by (56) (——).

and $\langle\phi_0|\phi_1'\rangle$ gives the same result. Moreover, by taking into account that a similar analysis in p-representation would give the correction of equation (54) but with q_0 in place of p_0, we expect that this correction corresponds to the error of ϕ_0 for large values of $|q|$. Then, we arrive at the conclusion that for q_0 and $p_0 \sim \sqrt{\hbar}$, a better estimation of the overlap is given by

$$\langle\phi|\phi'\rangle \sim \langle\phi_0|\phi_0'\rangle(1 - \beta T/\pi),$$

with[16]

$$\beta \equiv (\sqrt{q_0} + \sqrt{p_0})/2. \tag{55}$$

We stress that β is not a classical invariant but it depends on the particular surface of section selected for the calculation. However, in appendix A we show that after an integration along a direction transverse to the surface of section, the canonical invariance of matrix elements is restored. On the other hand, the particular value of β depends on the behaviour of ϕ near $q = 0$; so, if we use the integral representation $\tilde{\phi}$ (in place of ϕ), it is necessary to multiply the rhs of (55) by $\tilde{\Gamma}(1/4)/(\pi^{1/2}2^{1/4}) \simeq 1.720$.

It is evident that the previous approximation does not work for $A = O(1)$ because the overlap changes its sign; from equation (49) we observe that the correction ϕ_1 is simply responsible for the modulation of the oscillatory function. By taking into account this fact, it is reasonable to consider the previous correction as the first term in the expansion of a positive defined function; for instance, an exponential. Then, an estimation of the overlap, for $A > \hbar$, is given by[17]

$$\langle\phi|\phi'\rangle \sim \frac{2\sqrt{\pi}}{T}\frac{\cos(A/2\hbar)}{\sqrt{A/2\hbar}}\,\mathrm{e}^{-\beta T/\pi}. \tag{56}$$

Figure 4 compares, as a function of the heteroclinic area, a numerical evaluation of the overlap (according to (49)) with equation (56). We observe that they have the same oscillatory behaviour for $A > \hbar$, although there is some discrepancy between their amplitudes. In order to study such discrepancy, figure 5 shows the ratio between a numerical evaluation of $\langle\phi|\phi'\rangle$ and equation (56)[18]. From the figure, it is evident that equation (56) provides a good estimation of the order of magnitude and moreover, it is apparently an upper bound (as should be expected according to the used estimation for ϕ).

Now, we shall evaluate Hamiltonian matrix elements between scar functions. At this point, we stress that $\hat{H}$ is an approximation valid in the vicinity of the fixed point $(0, 0)$ and

[16] Note that $\beta = A^{1/4}$ for $q_0 = p_0$, and $\beta > A^{1/4}$ for $q_0 \neq p_0$.
[17] Recall that $T = |\ln\hbar|$.
[18] All numerical calculations are taken for $q_0 = p_0$.

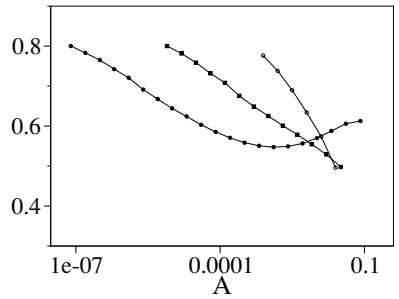

Figure 5. As a function of A, ratio between a numerical evaluation of the overlap (equation (49)) and the estimate given by (56), for $1/8\hbar = 10^3$ (○), $1/8\hbar = 10^5$ (■) and $1/8\hbar = 10^7$ (●).

its pieces of manifolds; see appendix B. In this sense, $\hat{H}$ cannot be applied to ϕ' and for this reason we impose the Hermitian property by the following definitions,

$$\langle\phi|\hat{H}_h|\phi'\rangle \equiv \tfrac{1}{2}[\langle\hat{H}\phi|\phi'\rangle + \langle\phi|\hat{H}'\phi'\rangle] \tag{57}$$

and $\langle\phi'|\hat{H}_h|\phi\rangle \equiv \langle\phi|\hat{H}_h|\phi'\rangle^*$. The operator $\hat{H}_h$, on the lhs of equation (57), is the so-called pure hyperbolic Hamiltonian in [6] (see appendix B for a detailed explanation). The action of $\hat{H}_h$ on scar functions is equivalent to the action of the Hamiltonian of the system $\hat{H}_{\rm sys}$ minus the energy E of the surface of section (which is equal to the Bohr–Sommerfeld energy of the scar functions ϕ and ϕ'); for instance, $\hat{H}_h|\phi\rangle \simeq (\hat{H}_{\rm sys} - E)|\phi\rangle$.

As $\phi(q)$ and $\mathrm{i}\hat{H}\phi(q)$ are even real functions, equation (57) can be written in the following way,

$$\langle\phi|\hat{H}_h|\phi'\rangle = \frac{-\mathrm{i}}{2}\int_{-\infty}^{\infty} f(q)\,\mathrm{e}^{\mathrm{i}p_0(q-q_0/2)/\hbar}\,\mathrm{d}q, \tag{58}$$

where the real function

$$f(q) = \mathrm{i}\hat{H}\phi(q-q_0)\phi(q) - \mathrm{i}\hat{H}\phi(q)\phi(q-q_0)$$

is evidently odd with respect to $q = q_0/2$. Then, the matrix element is

$$\langle\phi|\hat{H}_h|\phi'\rangle = \int_{q_0/2}^{\infty} f(q)\sin[p_0(q-q_0/2)/\hbar]\,\mathrm{d}q. \tag{59}$$

In the range $[q_0/2, \infty)$, $f(q)$ has a maximum at $q = q_0$; from equations (22), (23), (44) and (45), there results for $|q - q_0| \leqslant O(\hbar)$ and $q_0 \geqslant O(\sqrt{\hbar})$

$$f(q) \simeq \frac{2^{3/2}\pi^{1/2}\hbar^{1/2}[1 - (q-q_0)^2/10\hbar^2]\cos[\pi t_0(q_0)/T]}{T^2\sqrt{q_0}}. \tag{60}$$

On the other hand, for $|q - q_0| > O(\hbar)$ (using equations (44) and (45)) we have

$$f(q) \simeq \frac{\hbar\pi}{T^2}\frac{\sin[g(q)]}{\sqrt{|q|\,|q-q_0|}}, \tag{61}$$

where from equation (41)

$$g(q) = \frac{\pi}{T}[t_0(q) - t_0(q-q_0)] = \frac{\pi}{T}\ln\left(\frac{|q|}{|q-q_0|}\right).$$

Working as before in equation (52), we only consider the divergence at $q = q_0$ by using

$$f_0(q) = \frac{\hbar\pi}{T^2\sqrt{q_0|q-q_0|}}$$

in place of $f(q)$, and making the lower limit of integration in equation (59) equal to $-\infty$ as follows:

$$\langle\phi|\hat{H}_h|\phi'\rangle \sim \frac{\hbar\pi}{T^2\sqrt{q_0}}\int_{-\infty}^{\infty}\frac{\sin[p_0(q-q_0/2)/\hbar]\,\mathrm{d}q}{\sqrt{|q-q_0|}} = \frac{\hbar\pi^{3/2}}{T^2}\frac{\sin(A/2\hbar)}{\sqrt{A/2\hbar}}. \tag{62}$$

In the following, we analyse the error committed by using $f_0(q)$ in place of $f(q)$. First, we define the correction

$$f_1(q) = \frac{2^{3/2}\pi^{1/2}\hbar^{1/2}}{T^2\sqrt{q_0}} - \frac{\hbar\pi}{T^2\sqrt{q_0|q-q_0|}} \qquad \text{for} \quad |q-q_0| < q_1,$$

where $q_1 = \pi\hbar/8$, and $f_1(q) = 0$ otherwise. In this way, $f_0(q) + f_1(q)$ behaves like $f(q)$ near $q = q_0$ for $q_0 = O(\sqrt{\hbar})$ (see (60)), and $f_0(q) + f_1(q) \geqslant f(q)$ for all q. Then, the correction to the matrix element is given by

$$\int_{q_0-q_1}^{q_0+q_1} f_1(q)\sin[p_0(q-q_0/2)/\hbar]\,\mathrm{d}q \simeq -\frac{\hbar\pi^{3/2}}{T^2}\frac{\sin(A/2\hbar)}{\sqrt{A/2\hbar}}\frac{\sqrt{p_0}}{2}.$$

Using the same arguments given after equation (54), we arrive at the conclusion that this correction introduces the factor $\mathrm{e}^{-\beta}$.

Second, we have assumed that $\sin[g(q)] = 1$ (see (61)). In order to estimate the error of this approximation, we note that according to the factor $\sin[p_0(q-q_0/2)/\hbar]/\sqrt{|q-q_0|}$, the range q_2, around q_0, providing the main contribution to the integral satisfies $p_0q_2/\hbar \sim 1$. Then, taking into account that on the borders of this region we have $\sin[g(q_0 \pm q_2)] \simeq \sin[(\pi/T)\ln(A/\hbar)]$, a rough estimation of this correction can be given by a factor which is the mean value between the unity and $\sin[(\pi/T)\ln(A/\hbar)]$.

With the inclusion of these corrections, the Hamiltonian matrix element between scar functions takes the form

$$\langle\phi|\hat{H}_h|\phi'\rangle \sim \frac{\hbar\pi^{3/2}}{T^2}\frac{\sin(A/2\hbar)}{\sqrt{A/2\hbar}}\frac{\{1+\sin[(\pi/T)\ln(A/\hbar)]\}}{2}\,\mathrm{e}^{-\beta}. \tag{63}$$

We recall that equations (56) and (63) use the units chosen in section 2. In order to obtain these equations in arbitrary units, it is necessary to replace T for $\ln(QP/\hbar)$, β for $(\sqrt{q_0/Q} + \sqrt{p_0/P})/2$, and finally to include the factor λ on the rhs of equation (63). We would also like to point out that even though in our example of figure 3, the heteroclinic area is negative, the analysis for the positive case practically follows in the same way. In fact, by replacing the original hyperbolic Hamiltonian qp with $-qp$, the flux in figure 3 turns clockwise. Hence, the overlap does not change while the previous equation changes its sign. The two possibilities can be considered at the same time by making the following modification in equation (63):

$$\sin\left(\frac{A}{2\hbar}\right) \to -\sin\left(\frac{1}{2\hbar}\oint p\,\mathrm{d}q\right).$$

Figure 6 compares, as a function of A, a numerical evaluation of the Hamiltonian matrix element according to (59) with the estimate given by equation (63). We observe that they have the same oscillatory behaviour although there is some discrepancy between their amplitudes. In order to study such discrepancy, figure 7 shows the ratio between equations (59) and (63). From the figure, it is evident that (63) provides a very good estimate of the order of magnitude; in fact, according to the numerical calculation, this equation overestimates by around 25% the right value.

Finally, we would like to discuss the range of validity of equations (56) and (63). First, note that the proposed Hamiltonian approximation (see equation (B.1)) is local and restricted

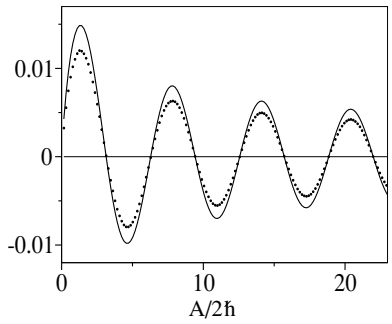

Figure 6. For $1/8\hbar = 10^5$, the plot compares as a function of $A/2\hbar$, a numerical evaluation of the Hamiltonian matrix element between scar functions divided by $\hbar$ ($\cdots\cdots$) according to (59), with the analytical estimation provided by equation (63) (——).

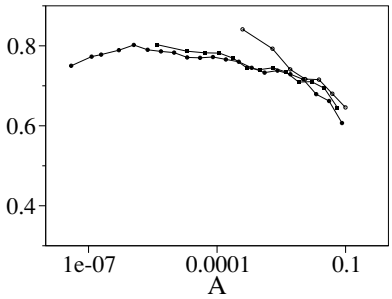

Figure 7. As a function of A, ratio between a numerical evaluation of the Hamiltonian matrix element according to (59) and the estimate given by (63), for $1/8\hbar = 10^3$ (○), $1/8\hbar = 10^5$ (■) and $1/8\hbar = 10^7$ (●).

to a limited region of phase space in the vicinity of the orbit. In particular, equation (1) is unable to reproduce the intersection of manifolds at homoclinic points. Of course, the same problem appears for the intersection of manifolds at heteroclinic points, the relevant points for the evaluation of matrix elements. For this reason, the intersection of manifolds at heteroclinic points is considered at quantum level by the overlap of suitable semiclassical wavefunctions. So, it should be clear that the obtained expressions are not restricted to those regions where the local approximation works but they are of general validity.

5. Conclusions

We have studied the asymptotic properties of scar functions on a Poincaré surface of section; that is, wavefunctions with hyperbolic structure living in a finite region of the $q-p$ plane. Then, we were able to obtain asymptotic estimates for the overlap between scar functions centred at different points of the $q-p$ plane, and also for the corresponding Hamiltonian matrix element. As a remarkable result, these matrix elements depend essentially on the heteroclinic area between pairs of fixed points.

According to equation (56), the overlap between scar functions tends to zero at least as $1/T$, where T is of the order of the Ehrenfest time. Here, we assume that the absolute value of the heteroclinic area satisfies $A > \hbar$, and this should be the case if we only consider short periodic orbits with periods no greater than the Ehrenfest time. On the other hand, from

equation (63) we observe that the product of a typical Hamiltonian matrix element by the energy density (which is of order $\hbar^{-2}$ for systems with two degrees of freedom) diverges in the semiclassical limit. These conclusions are relevant for the semiclassical description of chaotic eigenfunctions in terms of scar functions of short periodic orbits [13]. That is, we can say that the basis of scar functions is orthogonal in the semiclassical limit, and more importantly, this basis cannot be connected through perturbation theory to the set of eigenfunctions.

The dependence of matrix elements on the heteroclinic area shows two main characteristics. On the one hand, they are proportional to $1/\sqrt{A}$ and then, A defines a first ordering with respect to the interaction among periodic orbits. On the other hand, A imposes a rule of the Bohr–Sommerfeld type in the following sense: for $A = 2\pi\hbar(n + 1/2)$, where n is an integer, the Hamiltonian matrix element is maximum (in absolute value), while the overlap is zero. Moreover, the fact that Hamiltonian matrix elements are proportional to $\sin(A/2\hbar)$ means that each non-diagonal matrix element depends, in a very sensitive way, on the particular value of the corresponding heteroclinic area.

In appendix A we analyse the contribution to matrix elements from a direction transverse to the Poincaré surface of section when the two scar functions have the same mean energy, while the generalization for different mean energies is discussed in appendix C. The formulae in arbitrary units and including all the obtained contributions take the following form,

$$\langle a|b\rangle \sim \frac{2\sqrt{\pi}\,\mathrm{e}^{\mathrm{i}\alpha_{a,b}}}{T\sqrt{A/2\hbar}}\cos\left(\frac{1}{2\hbar}\oint p\,\mathrm{d}q\right)\exp\left[-\left(\frac{\Delta E}{2\sigma_T}\right)^2\right]N_{Ov} \tag{64}$$

and

$$\langle a|\hat{H}_{\mathrm{sys}} - \bar{E}|b\rangle \sim -\frac{\hbar\bar{\lambda}\pi^{3/2}\,\mathrm{e}^{\mathrm{i}\alpha_{a,b}}}{T^2\sqrt{A/2\hbar}}\sin\left(\frac{1}{2\hbar}\oint p\,\mathrm{d}q\right)\frac{\{1+\sin[(\pi/T)\ln(A/\hbar)]\}}{2}$$
$$\times\exp\left[-\frac{1}{2}\left(\frac{\Delta E}{2\sigma_T}\right)^2\right]N_{\mathrm{H}} \tag{65}$$

where $T = \ln(S/\hbar)$. The area S is a generalization of the area QP used in section 4. This area is an estimation of the region transverse to the periodic orbits where the semiclassical scar function construction works. A reasonable selection for S in terms of classical invariants is to take the minimum (or mean) value of the homoclinic areas related to the periodic orbits playing a role in the calculation; see appendix D.

Finally, we would like to state some remarks:

(a) Note that the only reference to the Poincaré surface of section of equations (64) and (65) is given through $\alpha_{a,b}$, by the selected phase convention of the scar functions at points a and b. Hence, we can say that these expressions are canonically invariants.

(b) As scar functions live in finite regions of phase space, matrix elements should tend to zero when the corresponding fixed points go away from one an other. We stress that such behaviour is taken into account by the factors $\mathrm{e}^{-\beta T/\pi}$ and $\mathrm{e}^{-\beta}$ of equations (56) and (63), respectively.

(c) When both POs have large period, several heteroclinic areas can be relevant for the evaluation of matrix elements. In such a case, as it was shown in appendix D, matrix elements consist of a sum of terms like those in equations (64) or (65).

(d) Direct interaction schemes like that of figure 11 are characterized by heteroclinic areas going to zero in the semiclassical limit[19]. In contrast, complex interaction processes like

[19] Take into account that the length of a typical PO in a scar function basis increases with $|\ln\hbar|$.

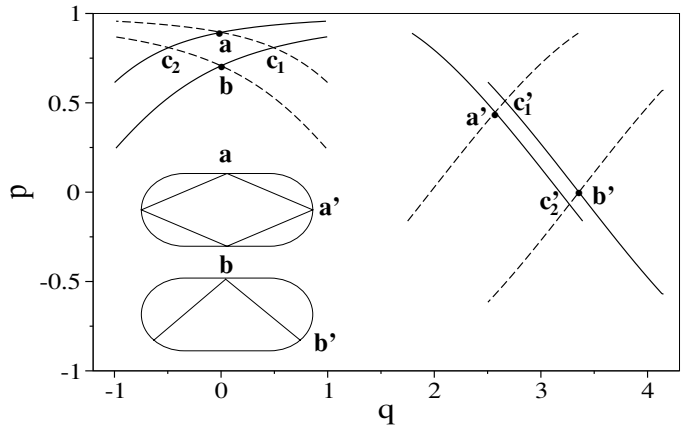

Figure 8. Poincaré surface of section on the boundary of the stadium billiard. We depict the behaviour of the stable (- - - -) and unstable (——) manifolds in the immediate vicinity of several fixed points (●) of the four bounces map. The intersecting points of the manifolds are labelled with c. The inset shows in configuration space the corresponding periodic orbits.

those of figure 12 (lower part), which are not included in our calculations, always involve the full phase space. For this reason, we are convinced that heteroclinic areas of direct processes play a central role in the semiclassical description of chaotic systems. In fact, the correlation between scar functions strongly depends on these areas for times lower than the Ehrenfest time, as it was shown in [14].

(e) Littlejohn evaluates overlaps for semiclassical wavefunctions related to intersecting Lagrangian manifolds [15]. His expression (see equation (2.16) in [15]) includes a Poisson bracket factor characterizing the intersection of manifolds, which is not present in our formulae. The reason is that for scar functions such Poisson bracket always takes the same value by construction. In fact, it can be written as the skew product of vectors ξ_s and ξ_u along the stable and unstable directions. Moreover the lengths of these vectors, which specify the density of the scar functions on the manifolds, are fixed by the relation $\xi_u \wedge \xi_s = J$ where J is the unity of angular momentum (see equation (11) in [6]).

Acknowledgments

We are really grateful to the referees for very helpful comments about the first version of this paper. This work was partially supported by SAB2002-22.

Appendix A

In this appendix, we discuss the validity of figure 3 for generic systems and the generalization of the phase convention used in section 4. Moreover, taking into account that section 4 only considers the contribution to matrix elements provided by a given Poincaré surface of section, we analyse the result of an integration in a direction transverse to the section.

First, let us consider as an introductory example two orbits of the stadium billiard which are periodic after four bounces with the boundary, as it is shown in the inset of figure 8. In this situation, all points indicated in the figure (a, a', b, and b') are fixed points of the map P^4,

where P is the Poincaré map in Birkhoff coordinates[20]. Therefore, the behaviour of the manifolds for these two selected periodic orbits can be analysed in the vicinity of the fixed points a and b, or equivalently in the vicinity of a' and b'; see figure 8. It is evident from the figure that the canonical transformation P yields the apparently complex picture shown in the vicinity of a and b, very much like the one presented in figure 3.

In the following, we will show that actually figure 3 describes the generic situation. To do this, we first recall that phase space is not a metric space; so, concepts like distances between points, angles between intersecting lines, or curvature of lines are misleading. The only properties of the Poincaré surface of section, invariant with respect to canonical transformations are (i) the symplectic area defined by a closed line and (ii) the intersection of lines. On the other hand, in chaotic systems there are two types of time-invariant lines on the Poincaré section; stable and unstable manifolds. Moreover, manifolds of the same type do not intersect; we can roughly say that they are parallel.

Taking into account the previous comments, figure 3 is equivalent to a generic picture, when they are compared with a symplectic structure. Therefore, there should exist a canonical transformation connecting both situations[21].

Now, let us analyse the behaviour of matrix elements under the action of canonical transformations. For simplicity, we first consider the estimate proposed in equation (53) for the evaluation of overlaps. As discussed previously, there is a canonical transformation connecting the points $(0, 0)$, (q_0, p_0), $(0, p_0) \equiv z_1$ and $(q_0, 0) \equiv z_2$ of figure 3, with the points a, b, c_1 and c_2 of figure 8, respectively. Moreover, the transformation can be approximated in the vicinity of z_1 and z_2 by symplectic transformations S_1 and S_2, respectively. Hence, the following relations follow,

$$|\langle a|c_j\rangle\langle c_j|b\rangle| \simeq |\langle\phi_0|z_j\rangle\langle z_j|\phi_0'\rangle| \simeq 2(\pi\hbar/A)^{1/2}/T \qquad \text{for} \quad j = 1, 2 \tag{A.1}$$

where $|c_j\rangle \equiv \hat{U}_j|z_j\rangle$. The unitary operator $\hat{U}_j$, which is the quantum counterpart of S_j, results from the combination of a Heisenberg operator with a metaplectic one [12].

Then, the overlap between the scar functions related to the fixed points a and b takes the form (we omit constant factors which are irrelevant in the present discussion)

$$\langle a|b\rangle \sim (\mathrm{e}^{\mathrm{i}\alpha_1} + \mathrm{e}^{\mathrm{i}\alpha_2})(\hbar/A)^{1/2}/T \tag{A.2}$$

with the phase α_j being the difference of phases of the scar functions at c_j. That is,

$$\alpha_1 = \frac{1}{\hbar}\left[\left(S_b + \int_b^{c_1} p\,\mathrm{d}q\right) - \left(S_a - \int_{c_1}^{a} p\,\mathrm{d}q\right)\right] = \frac{1}{\hbar}\left(S_b - S_a + \int_b^{a} p\,\mathrm{d}q\right) \tag{A.3}$$

and

$$\alpha_2 = \frac{1}{\hbar}\left[\left(S_b - \int_{c_2}^{b} p\,\mathrm{d}q\right) - \left(S_a + \int_a^{c_2} p\,\mathrm{d}q\right)\right] = \frac{1}{\hbar}\left(S_b - S_a - \int_a^{b} p\,\mathrm{d}q\right) \tag{A.4}$$

where the phases $S_a/\hbar$ and $S_b/\hbar$ at the corresponding fixed points are selected by convention, and the line integrals are taken along the pieces of manifolds following the flux direction on the manifolds; in our example it is anticlockwise. Hence, by substituting equations (A.3) and (A.4) in (A.2), there results

$$\langle a|b\rangle \sim \mathrm{e}^{\mathrm{i}\alpha_{a,b}} \cos\left(\frac{1}{2\hbar}\oint p\,\mathrm{d}q\right)(\hbar/A)^{1/2}/T \tag{A.5}$$

[20] The position q on the boundary is such that $q_a = 0$ and $q_{a'} = 1 + \pi/2$. Moreover, p is the fraction of momentum tangent to the boundary; so $|p| < 1$.

[21] The essence of this argument results more intuitively in the three-dimensional Euclidean space, where translations and rotations are the unique transformations keeping invariant the metric structure and the orientation of the space. Hence, rigid bodies being invariant with respect to translations and rotations, if two rigid bodies are equivalent there exists a translation plus a rotation connecting them.

where

$$\alpha_{a,b} \equiv \frac{1}{\hbar}\left(S_b - S_a + \frac{1}{2}\int_b^a p\,\mathrm{d}q - \frac{1}{2}\int_a^b p\,\mathrm{d}q\right). \tag{A.6}$$

This expression for the overlap is equivalent to equation (51). Note that in section 4 we have selected a phase convention (see equation (51)) to obtain real matrix elements; in the same way, we can select $S_b - S_a$ in order to satisfy $\alpha_{a,b} = 0$. However, it should be clear that in general it is impossible to verify this phase condition for all matrix elements of a scar function basis; so overlaps and Hamiltonian matrix elements have to include, in general, the phase $\alpha_{a,b}$ provided in equation (A.6).

Let us study whether there is a simple relation between $\alpha_{a,b}$ and the corresponding phase $\alpha_{a',b'}$, defined in the vicinity of a' and b'. First, note that the intersecting points c_1 and c_1' belong to the same heteroclinic orbit. Specifically, let ζ_a and ζ_b be finite sequences of symbols labelling the corresponding periodic orbits. Hence, c_1 and c_1' belong to the heteroclinic orbit[22] $\zeta_b^\infty\zeta_a^\infty$, while c_2 and c_2' belong to $\zeta_a^\infty\zeta_b^\infty$. Therefore, α_1 and α_2 are constant values because the phase increment of the two scar functions is given by the same line integral $\int p\,\mathrm{d}q/\hbar$ along the corresponding heteroclinic orbit. In particular, $\alpha_{a,b} = (\alpha_1 + \alpha_2)/2$ is also a constant value and then $\alpha_{a,b} = \alpha_{a',b'}$.

From the previous discussion, we arrive at the conclusion that each term on the rhs of equation (A.2) is a constant value. So in order to evaluate, for instance, the contribution of the first term in a direction transverse to the section, we simply integrate this constant value along the corresponding heteroclinic orbit. At this point, there is apparently a problem because $\zeta_b^\infty\zeta_a^\infty$ is not periodic and consequently the integral diverges. The origin of this problem is related to the approximation used in equation (A.1). The functions $\phi_0(q)$ and $\phi_0'(q)$, introduced in equation (50), are right solutions if the pieces of manifolds in figure 3 go to infinity. However, as we saw in equation (56), when the pieces of manifolds are limited to a finite range, the parameter β is relevant. This parameter is not invariant with respect to canonical transformations; hence, the overlap at different transverse sections takes in principle different values.

To clarify the situation, let us come back to figure 8 by introducing the Euclidean distance $d(\,,\,)$ in the plane q–p; of course, our conclusions do not depend on the particularly used metric. Note that $d(a, c_1) \simeq d(b, c_1)$ while $\gamma\, d(a', c_1') \simeq d(b', c_1')/\gamma$, where γ is a stretching factor; $\gamma \sim \mathrm{e}^{\tilde{\lambda}}$ with $\tilde{\lambda}$ the Lyapunov exponent per bounce. So, the parameter β increases by around the factor[23] $(\sqrt{\gamma} + 1/\sqrt{\gamma})/2$ when c_1 evolves towards c_1', and the same happens when c_1 evolves by the application of P^{-1}. Therefore, we can say that there is a point on the heteroclinic orbit (in our example it is c_1) where β takes its minimum value, $\beta = A^{1/4}$, and the Poincaré contribution to the first term of the overlap is maximum. Moreover, as c_1 evolves forwards or backwards in time, β increases according to the relation

$$\beta(t) \simeq A^{1/4}(\mathrm{e}^{\lambda t/2} + \mathrm{e}^{-\lambda t/2})/2 = A^{1/4}\cosh(\lambda t/2) \tag{A.7}$$

with λ the Lyapunov exponent per unit time. Hence, the transverse contribution to the first term is provided by the following well-behaved factor

$$N_{Ov} \equiv \int_{-\infty}^{\infty} \frac{\mathrm{e}^{-\beta(t)T/\pi}}{\sqrt{T_a T_b}}\,\mathrm{d}t \simeq \int_{-\infty}^{\infty} \frac{\exp[-(A^{1/4}T/\pi)\cosh(\lambda t/2)]}{\sqrt{T_a T_b}}\,\mathrm{d}t \tag{A.8}$$

[22] This orbit is the simplest one that converges to ζ_a (ζ_b) when the system evolves forwards (backwards) in time. In general, cycle permutations of the sequences ζ_a and ζ_b define different heteroclinic orbits $\zeta_b^\infty\zeta_a^\infty$; see appendix D where an example clarifies this point.

[23] An estimate for β is given by $(\sqrt{d(a, c_1)} + \sqrt{d(b, c_1)})/2$.

where T_a and T_b are the periods of the periodic orbits related to a and b, respectively[24]. Of course, the integration along the other heteroclinic orbit, in order to evaluate the transverse contribution of the second term of equation (A.2), is equal to the previous one. So, by substituting $e^{-\beta T/\pi}$ for N_{Ov} in equation (A.8), the overlap takes into account the transverse direction to the Poincaré section.

In the case of Hamiltonian matrix elements, the same analysis follows with $e^{-\beta}$ in place of $e^{-\beta T/\pi}$. Hence, the factor to be included in equation (63), in place of $e^{-\beta}$, results in

$$N_H \equiv \int_{-\infty}^{\infty} \frac{e^{-\beta(t)}}{\sqrt{T_a T_b}}\,dt \simeq \int_{-\infty}^{\infty} \frac{\exp[-A^{1/4}\cosh(\lambda t/2)]}{\sqrt{T_a T_b}}\,dt. \tag{A.9}$$

We would like to stress that for the most interesting cases, the previous factors are very insensitive to the involved parameters. For instance, let us consider short periodic orbits with periods of the order of the Ehrenfest time (the typical case); that is, $T_a, T_b \sim |\ln\hbar|/2\lambda$. Then, for strong interactions corresponding to $A \sim \hbar$, equations (A.8) and (A.9) become, in leading order, equal to 2, and for intermediate interactions ($A \sim \sqrt{\hbar}$) they become equal to 1.[25] This interaction scheme is discussed in the baker's map in appendix D.

Appendix B

In this appendix, we discuss the scar function construction for two degrees of freedom Hamiltonian systems, and the accuracy of the local Hamiltonian approximation used for the evaluation of Hamiltonian matrix elements.

Let γ be an unstable periodic orbit with period T and the Maslov index μ, and let x and y be curvilinear coordinates in configuration space along and transverse to γ, respectively. We use a synchronized (or adiabatic) motion approximation [6] where the fast motion along γ is decoupled from the slow transverse one. In this approximation, all the orbits in the vicinity of γ move in phase space with the same value of the variables x and p_x. Moreover, by virtue of Floquet's theorem the transverse motion, defined by y and p_y, is decomposed into one of periodic nature and another of hyperbolic character. Therefore, the Hamiltonian takes the form

$$H_{\rm sys}(x, p_x, y, p_y) \simeq H_{\parallel}(x, p_x) + H_p(y, p_y, x) + H_h(y, p_y, x). \tag{B.1}$$

The variable x appearing in H_p and H_h works as a parameter and plays the role of the time; so both transverse Hamiltonians depend periodically on the time with period T.

We emphasize that the Hamiltonian on the rhs of equation (B.1) is unbounded; that is, manifolds go away from the central orbit indefinitely. Hence, this approximation describes correctly the exponential divergence but eliminates the mixing property. On the other hand, the behaviour of the manifolds, while they go away from γ, can be described with arbitrary precision. In particular, a quadratic transverse Hamiltonian is sufficient for the description of their linear behaviour [6].

The restricted Hamiltonian $H_{\parallel}(x, p_x) + H_p(y, p_y, x)$ takes into account the topology of the orbits in the vicinity of γ. The motion described by this contribution is neutral and all the neighbouring orbits are periodic. When μ is even, these orbits have period T and take $\mu/2$ turns around γ. For μ odd, the neighbouring orbits, of period $2T$, give μ turns around γ.

Of course, these neighbouring closed paths (periodic orbits of the restricted Hamiltonian) are not classical trajectories of the full Hamiltonian $H_{\parallel} + H_p + H_h$. However, we remark that

[24] The factor $1/\sqrt{T_a T_b}$ normalizes the scar functions in the direction transverse to the Poincaré section.

[25] We used the asymptotic approximation $\int_{-\infty}^{\infty} \exp[-\alpha\cosh(x)]\,dx \simeq \log(1/\alpha^2)$, which is valid for $0 < \alpha \ll 1$. Moreover, the expression $\log(1 + 1.260947/\alpha^2)$ works satisfactorily up to $\alpha \sim 1$, and the expression $(1 - 1/8\alpha)\sqrt{2\pi/\alpha}e^{-\alpha}$ works for $\alpha > 1$.

this family of closed paths is invariant with respect to the full evolution; that is, a periodic orbit of $H_{\|} + H_p$ evolves with the Hamiltonian $H_{\|} + H_p + H_h$ within the family of periodic orbits of $H_{\|} + H_p$. Therefore, the time evolution of these closed paths can be analysed by the evolution of their intersecting points with a transverse surface of section defined at a given value x_0. In such a case, the evolution of the closed paths is taken into account by $H_h(y, p_y, x_0)$. It should be clear that this evolution is right in those regions of phase space where the manifolds resulting from $H_{\|} + H_p + H_h$ provide a good approximation to the actual manifolds of γ.

To clarify the previous picture, let us consider the Hamiltonian $H(x, p_x, y, p_y) = p_x^2 + x^2 + p_y^2 - y^2$. This unbounded Hamiltonian only contains one periodic orbit at each given energy, defined by the condition $p_y = y = 0$. As the mixing property is not present in this Hamiltonian, the approximation provided by equation (B.1) is actually exact. Moreover, the implied decomposition is given by $H_{\|}(x, p_x) = p_x^2 + x^2$, $H_p(y, p_y, x) = 0$ and $H_h(y, p_y, x) = p_y^2 - y^2$.[26] Note that $H_p = 0$ because the topology of the neighbouring orbits is trivial in this example; the stable (unstable) manifold is defined by the relation $p_y = -y$ ($p_y = y$) when observed at an arbitrary value x_0.

The motion of the restricted Hamiltonian $H_{\|} + H_p = p_x^2 + x^2$ consists of periodic orbits equivalent to the central one, but where the transverse variables are shifted from $p_y = y = 0$ to arbitrary values $p_y = p_0$ and $y = y_0$ specifying the given orbit. The important point to be noted is that these closed paths, or equivalently these periodic orbits of the restricted Hamiltonian, evolve under the action of the full Hamiltonian in a trivial way. The motion of the variables x and p_x is unaffected by the inclusion of H_h, so a closed path evolves according to a translation along the transverse directions. In this way, periodic orbits of $H_{\|} + H_p$ evolve to other ones, and this evolution is governed by H_h.

Now, we come back to the general discussion by mentioning that these neighbouring closed paths are the classical objects on which we semiclassically construct scar functions [6]. For instance, let us consider a bunch of closed paths of width $\sqrt{\hbar}$ around γ. When looked at on a transverse surface of section defined by $x = x_0$, these paths cross the section at a given set of points on the plane y–p_y. Correspondingly, the semiclassical construction consists of (i) a local plane-wave approximation along the bunch of closed paths with energy equal to the energy of γ (so, the possible energies of γ must satisfy a quantization condition of the Bohr–Sommerfeld type), and (ii) a transverse wave packet related to the set of intersecting points in such a way that its evolution is described by the quantum version, $\hat{H}_h$, of $H_h(y, p_y, x_0)$. Hence, by evolving the transverse wave packet with $\hat{H}_h$, the scar state, $|\phi\rangle$, can be constructed as explained in section 3. Moreover, the action of $\hat{H}_h$ on $|\phi\rangle$ provides a good local approximation for the action of the quantum Hamiltonian of the system

$$\hat{H}_h|\phi\rangle \simeq (\hat{H}_{\rm sys} - E)|\phi\rangle \tag{B.2}$$

where E is the energy of γ. This relation results from the fact that $|\phi\rangle$ is constructed with periodic orbits of $H_{\|} + H_p$, and then $(\hat{H}_{\|} + \hat{H}_p)|\phi\rangle \simeq E|\phi\rangle$.

Equation (B.2) is the starting point for the evaluation of Hamiltonian matrix elements. When two periodic orbits live in a common region of phase space, there exists a suitable surface of section where the vicinity of these orbits can be represented by figure 3. Hence, the expressions derived in section 4 are justified.

However, we emphasize that this approach contains an essential error. The application of $\hat{H}_h$ on $|\phi\rangle$ uses the knowledge of the position of the corresponding fixed point; but such information should be restricted at quantum level by the uncertainty principle. Therefore, the local Hamiltonian approximation incorporates a harmful classical ingredient that destroys the

[26] In the generic case, H_h (and also H_p) is a polynomial with coefficients being functions of x.

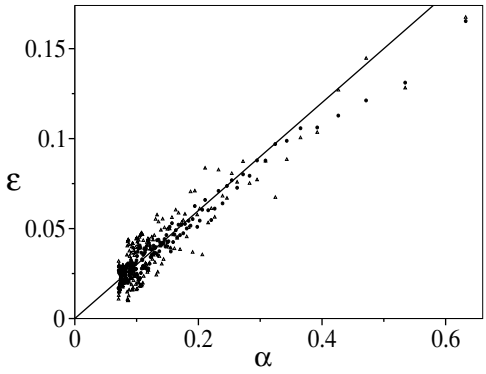

Figure 9. Relative level of non-Hermiticity, $\mathcal{E}$, of Hamiltonian matrix elements between scar functions according to equation (B.3), as a function of $\alpha \equiv (2\pi\hbar/A)^{1/2}$. For $1/8\hbar = 10^7$ (●), and for $1/8\hbar = 10^5$ (△). The straight line satisfies the relation $\mathcal{E} = 0.3\,\alpha$.

Hermitian property of the operator. This is the price we have to pay for reducing the dynamical information to the immediate vicinity of an orbit.

An estimate of this error can be obtained by simple arguments. The uncertainty of the fixed point (q_0, p_0) (see figure 3) being around $\sqrt{\hbar}$ for each variable, the relative error of the heteroclinic area A is $\sim \sqrt{\hbar/A}$. So, as Hamiltonian matrix elements essentially depend on A, their relative error should also be $\sim\sqrt{\hbar/A}$. In order to verify this prediction, we note that a measure of the relative error is given by the level of non-Hermiticity of matrix elements (the notation of section 4 is used)

$$\mathcal{E}(A) \equiv \frac{|\langle\hat{H}\phi|\phi'\rangle - \langle\phi|\hat{H}'\phi'\rangle|_{\text{mean}}}{|\langle\hat{H}\phi|\phi'\rangle + \langle\phi|\hat{H}'\phi'\rangle|_{\text{mean}}}. \tag{B.3}$$

Taking into account that numerator and denominator are oscillatory functions of $A/2\hbar$, we consider mean values over the range $[A/2\hbar - \pi/2,\, A/2\hbar + \pi/2]$. Figure 9 depicts $\mathcal{E}$ as a function of $\alpha \equiv (2\pi\hbar/A)^{1/2}$, for two different values of $\hbar$, showing that the relation $\mathcal{E} \sim 0.3\ \alpha$ works.

Finally, it is worth mentioning that the recipe given by equation (57) imposes the Hermitian property on Hamiltonian matrix elements. We hope that this trick reduces the discussed error; numerical studies in billiards or maps should shed light on this point. However, we note that this error is not a serious problem for the evaluation of matrix elements between scar functions of short periodic orbits because in such a case, the heteroclinic area is greater than $\hbar$.

Appendix C

We will evaluate matrix elements between the scar functions ϕ and ϕ', with mean energies E and E', respectively; these energies are the so-called Bohr–Sommerfeld energies in [6]. Taking into account that each scar function lives on a given energy shell, it is reasonable to hope that matrix elements decrease as the corresponding energy shells go away from one another. Even though this is a simple and clear picture, the arguments used in this appendix are of quantum nature because we have a deep knowledge of the spectral behaviour of scar functions.

In section 4, we used the same stability index λ for the two fixed points because all equations derived in the paper use λ^{-1} as the unity of time; so λ is not explicitly present in

those equations. Here, arbitrary units are used and consequently, we admit different stability indices λ and λ' for the periodic orbits associated with ϕ and ϕ', respectively. Then, the energy dispersions of ϕ and ϕ' are given in leading order by $\sigma \simeq \lambda\pi\hbar/|\ln\hbar|$ and $\sigma' \simeq \lambda'\pi\hbar/|\ln\hbar|$.

We note that according to the meaning of energy dispersion, the overlap $\langle\phi|\phi'\rangle$ should be practically zero for $|\Delta E| \gg \sigma_T$, where $\Delta E \equiv E - E'$ and $\sigma_T \equiv \sqrt{\sigma^2 + \sigma'^2}$. Of course, such a situation is not taken into account neither in (56) nor in (A.8) because they were derived for $\Delta E = 0$.

In order to solve the question, it is worth emphasizing that scar functions are constructed by using an adiabatic approximation for the motion in the vicinity of the periodic orbit, where the slow transverse motion is decoupled from the fast one along the orbit; see appendix B for a detailed discussion. Within the same approximation, the overlap is decoupled into two factors related to the corresponding motions. Hence, the slow transverse motion is given by the contribution on the surface of section (see equation (56)), with an energy section equal to $\bar{E} \equiv (E + E')/2$.[27] On the other hand, we hope that the factor related to the fast motion (transverse to the section) has a smooth dependence on ΔE. As equation (A.8) provides the contribution transverse to the surface of section when $\Delta E = 0$, we analyse the required modification for $\Delta E \neq 0$.

Taking into account that the overlap can be written in the basis of eigenfunctions of the system as $\langle\phi|\phi'\rangle = \sum_\mu \langle\phi|\phi_\mu\rangle\langle\phi_\mu|\phi'\rangle$, the smooth dependence on ΔE should be related to the smoothed distributions of $|\langle\phi|\phi_\mu\rangle|$ and $|\langle\phi'|\phi_\mu\rangle|$.[28] For distributions living in the same energy region, the factor is close to the unity, and when they are far away the factor should be around zero.

In equation (20) there is information about the smoothed distribution of the square modulus of the amplitudes in the basis of eigenfunctions. However, we stress that a detailed numerical study in a realistic system (the Bunimovich stadium billiard) shows that a scar function is distributed in the spectrum, following a Gaussian distribution with second momentum given by equation (20). Evidently, higher even momenta are not well described by (20) because, for instance, the 4-momentum of the Gaussian distribution is $3\sigma^4$. This means that equation (20) provides the right $|\ln\hbar|$ order for all n, but the precise value only for the second momentum. This discrepancy is related to the mixing property of chaotic systems because in our derivation of equation (20), we have not considered the intersection of the manifolds.

In conclusion, according to the previous discussions we propose the following expression for the overlap between scar functions with different mean energies

$$\langle\phi|\phi'\rangle_{(\Delta E)} \simeq \exp\left[-(\Delta E/2\sigma_T)^2\right]\langle\phi|\phi'\rangle. \tag{C.1}$$

The factor $\exp[-(\Delta E/2\sigma_T)^2]$ results from the overlap of two Gaussian distributions with dispersions $\sqrt{2}\sigma$ and $\sqrt{2}\sigma'$, which describe the smoothed distributions of $|\langle\phi|\phi_\mu\rangle|$ and $|\langle\phi'|\phi_\mu\rangle|$ respectively.

In the same way, we propose the following expression for the Hamiltonian matrix element between scar functions with different mean energies:

$$\langle\phi|\hat{H}_{\rm sys} - \bar{E}|\phi'\rangle_{(\Delta E)} \simeq \exp\left[-\tfrac{1}{2}(\Delta E/2\sigma_T)^2\right]\langle\phi|\hat{H}_h|\phi'\rangle. \tag{C.2}$$

On the lhs of the previous equation, we have included the energy $\bar{E}$, in place of E or E', in order to impose the Hermitian property to $\hat{H}_{\rm sys}$. On the rhs of equation (C.2), the factor $1/2$ inside the exponential has taken into account the fact that the dispersion of $|\langle\phi_\mu|\hat{H}\phi\rangle|$ is

[27] We note that the representation of scar functions on the surface of section is unchanged by energy variations of the order of dispersion. In this respect, the evaluation of equation (56) is practically the same at energies of the section equal to E, E' or $\bar{E}$.

[28] The strong correlation between the amplitudes $\langle\phi|\phi_\mu\rangle$ and $\langle\phi_\mu|\phi'\rangle$ is taken into account by the contribution on the section.

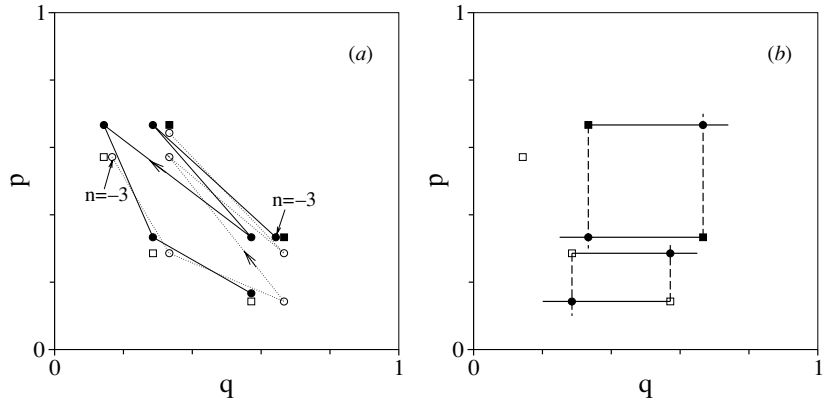

Figure 10. The periodic orbits $(01)^\infty$ and $(001)^\infty$ of the baker's map are indicated with ■ and □, respectively. (*a*) Six consecutive points of the heteroclinic orbits $(01)^\infty(001)^\infty$ and $(001)^\infty(01)^\infty$ are also depicted in (●) and (○), respectively; starting at $n = -3$ solid and dotted lines help to follow the corresponding sequence. (*b*) Homoclinic areas related to each periodic orbit with the corresponding relevant homoclinic points (●).

$\sqrt{3}$ times the dispersion of $|\langle\phi|\phi_\mu\rangle|$ (and the same for ϕ'). Finally, the factor $\langle\phi|\hat{H}_h|\phi'\rangle$ is the one corresponding to $\Delta E = 0$, with stability index $\bar{\lambda} = (\lambda + \lambda')/2$ in order to impose again the Hermitian property on matrix elements.

Appendix D

In this appendix, we clarify with an example the interaction picture described in the second part of appendix A. Moreover, we analyse the involved approximation by considering figure 3 as the unique relevant mechanism of interaction.

In order to simplify the discussion we have selected the baker's map as our dynamical system. The phase space of the map is the square $0 \leqslant q < 1, 0 \leqslant p < 1$. By using a binary expansion of these coordinates, as $q = \cdot a_0 a_1 a_2 \ldots$ and $p = \cdot a_{-1} a_{-2} a_{-3} \ldots$ ($a_j = 0$ or 1), a point of phase space can be represented by a doubly infinite binary sequence

$$(q, p) = \ldots a_{-3} a_{-2} a_{-1} \cdot a_0 a_1 a_2 \ldots .$$

Then, the action of the map over (q, p) is specified by a right-shift of the central dot, which identifies the present position on the orbit. When the central dot is not included, we simply refer to the orbit as a geometrical object.

Let us consider the interaction of POs with different period in order to show that the description of appendix A can be applied to general pair of POs. The only primitive PO of period 2 consists of the points $(1/3, 2/3)$ and $(2/3, 1/3)$, and it is represented by the infinite sequence $\ldots 010101 \ldots \equiv (01)^\infty$, while the PO of period 3 with symbol $(001)^\infty$ contains the points $(1/7, 4/7)$ $(2/7, 2/7)$ and $(4/7, 1/7)$. In figure 10(*a*) these POs are shown with ■ and □, respectively; moreover, the most relevant heteroclinic orbits contributing to the interaction between these POs are plotted with circles. The point $(1/7, 2/3) = \ldots 0101 \cdot 001001 \ldots = (01)^\infty \cdot (001)^\infty$ corresponds to the simplest heteroclinic orbit that goes from $(01)^\infty$ to $(001)^\infty$ and six consecutive points of this orbit are indicated with ●. Equivalently, the point $(1/3, 4/7) = (001)^\infty \cdot (01)^\infty$ corresponds to the simplest heteroclinic orbit that goes from $(001)^\infty$ to $(01)^\infty$ and also six consecutive points are indicated with (○). On the other hand, figure 10(*b*) indicates with ● the pair of homoclinic points $(2/3, 2/3) = (01)^\infty \cdot (10)^\infty$ and

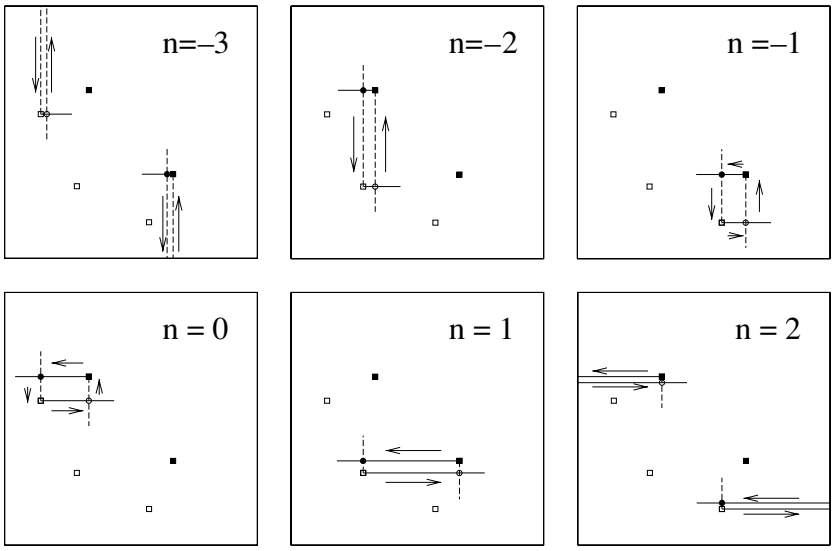

Figure 11. Six consecutive steps of the most relevant interaction scheme between the POs $(01)^\infty$ and $(001)^\infty$ are depicted. This scheme is constructed with the heteroclinic orbits shown in figure 10(*a*). The corresponding heteroclinic area is $-8/441$.

$(1/3, 1/3) = (10)^\infty \cdot (01)^\infty$ related to $(01)^\infty$, and the pair $(4/7, 2/7) = (010)^\infty \cdot (100)^\infty$ and $(2/7, 1/7) = (100)^\infty \cdot (010)^\infty$ related to $(001)^\infty$. Each pair of points defines a homoclinic area, with absolute value S being an estimate of the area QP of section 4 where each scar function is constructed. In our simplified model of section 4 the area QP is the same for the two POs, so an estimate of this area can be the minimum absolute value of the two homoclinic areas indicated in the figure; that is, $S = 2/49$.

The most important point to be noted is that each pair of heteroclinic orbits defines univocally a given interaction picture. For instance, figure 11 follows the interaction scheme related to the previously mentioned heteroclinic orbits during six steps. This figure shows clearly that an interaction picture is not of periodic nature, but of hyperbolic character. That is, there is a time n_0 (in our example between $n = -1$ and $n = 0$) where the interacting rectangle reduces to a square, while for times going away from n_0 the rectangle departs more and more from a square shape. We can roughly say that the interaction is specified by a tube with fixed transverse area but where its shape changes strongly as it departs from a given transverse position.

The pieces of manifolds of figure 11 are of two types. At $n = -2, -1, 0$ and 1 they always go away from the corresponding fixed point, while at $n = -3$ and 2 there are pieces of manifold that abandon the interaction region and later come back to it. Evidently, the last situation cannot be reproduced by the Hamiltonian approximation discussed in appendix B, which only describes manifolds that go away from a fixed point. However, it should be clear that the interaction at $n = -3$ or $n = 2$ is completely equivalent to the other situations. That is, the interacting scheme consists of a rectangle defined by the periodic and heteroclinic orbits. So the same formulae derived for cases like those at $n = -2, -1, 0$ and 1 should be right for other situations like those at $n = -3$ or $n = 2$; in fact, canonical transformations connect the different pictures. Of course, the contribution to matrix elements at $n = -3$ or $n = 2$ has to be much smaller than at $n = -1$ or $n = 0$ because scar functions are limited in extension by the homoclinic areas shown in figure 10(*b*). But this fact is taken into account by

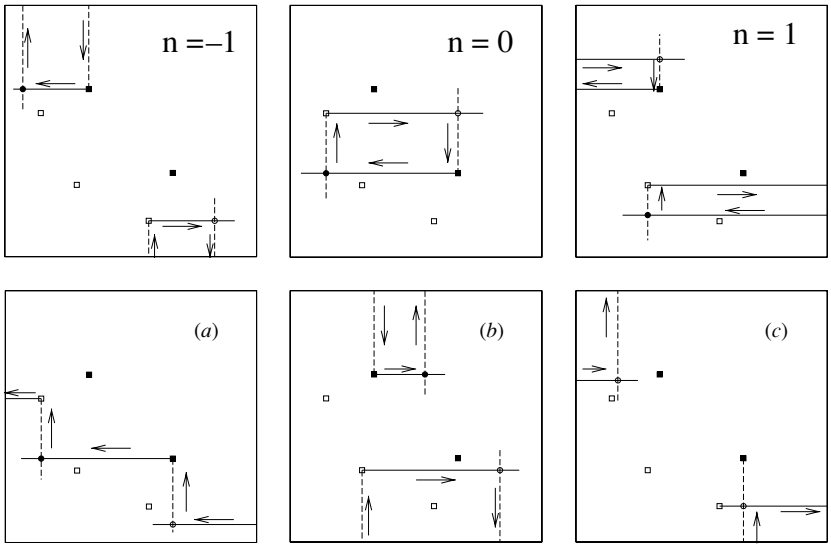

Figure 12. Upper panels: interaction scheme corresponding to the heteroclinic orbits with position at time $n = 0$ given by $(2/3, 4/7) = (001)^\infty \cdot (10)^\infty$ and $(1/7, 1/3) = (10)^\infty \cdot (001)^\infty$. The corresponding heteroclinic area is $55/441$. Lower panels: interaction schemes related to the heteroclinic points (*a*) $(2/3, 1/14) = (100)^\infty 0 \cdot (10)^\infty$ and $(1/7, 1/3) = (10)^\infty \cdot (001)^\infty$, (*b*) $(5/6, 2/7) = (010)^\infty \cdot 1(10)^\infty$ and $(15/28, 2/3) = (01)^\infty \cdot 10(001)^\infty$, and (*c*) $(2/3, 1/7) = (100)^\infty \cdot (10)^\infty$ and $(1/6, 9/14) = (010)^\infty 1 \cdot 0(01)^\infty$.

our formulae because $\beta(n) \simeq (A/S)^{1/4} \cosh[\lambda(n - n_0)/2]$ (see (A.7)), and the contribution to matrix elements decays exponentially with β; that is, exponentially with an exponential of $|n - n_0|$ (see equations (A.8) and (A.9)). Here, $A = 8/441$ is the absolute value of the heteroclinic area corresponding to this interaction scheme.

The upper part of figure 12 shows another interaction scheme corresponding to the heteroclinic orbits with position at $n = 0$ given by $(1/7, 1/3) = (10)^\infty \cdot (001)^\infty$ and $(2/3, 4/7) = (001)^\infty \cdot (10)^\infty$. The heteroclinic area related to this interaction scheme is around seven times greater than the heteroclinic area of figure 11. So, taking into account that the maximum contribution to matrix elements (it occurs for $n = n_0$) is proportional to $\exp[-(A/S)^{1/4}|\ln\hbar|/\pi]/\sqrt{A}$ for overlaps and to $\exp[-(A/S)^{1/4}]/\sqrt{A}$ for Hamiltonian matrix elements, it is clear that the contribution related to figure 11 is the most relevant one. Specifically, the ratio between the contributions related to figures 11 and 12 (upper part) is $\sim 2.6/\hbar^{0.16}$ for the overlap and ~ 4.3 for the Hamiltonian matrix element. On the other hand, it should be clear that the contribution provided by the upper part of figure 12 can also be considered by using exactly the same formulae. So the evaluation of matrix elements simply results by adding the contributions provided by all direct interaction schemes like that of figures 11 and 12 (upper part). In our example, there is one more interaction scheme (with the same heteroclinic area of figure 12, upper part) which satisfies the formulae of section 4; it is defined by the heteroclinic points $(4/7, 2/3) = (01)^\infty \cdot (100)^\infty$ and $(1/3, 1/7) = (100)^\infty \cdot (01)^\infty$.

On the other hand, there is an infinite number of interaction schemes which cannot be described by our formulae. They are characterized by complex heteroclinic orbits; that is, heteroclinic orbits where the transition from one PO to the other includes an intermediate excursion to other places of phase space. For instance, in figure 12

(lower part) we depict three of these schemes (the simplest ones) related to the heteroclinic points: (*a*) $(2/3, 1/14) = (100)^\infty 0 \cdot (10)^\infty$ and $(1/7, 1/3) = (10)^\infty \cdot (001)^\infty$, (*b*) $(5/6, 2/7) = (010)^\infty \cdot 1(10)^\infty$ and $(15/28, 2/3) = (01)^\infty \cdot 10(001)^\infty$, and (*c*) $(2/3, 1/7) = (100)^\infty \cdot (10)^\infty$ and $(1/6, 9/14) = (010)^\infty 1 \cdot 0(01)^\infty$. Evidently, the contribution provided by each one of these complex schemes is smaller than that related to a direct process because they always contain pieces of manifolds which are of the order 1. This is a strong difference with respect to direct interaction schemes as described above, where the pieces of manifolds defining the rectangles can be arbitrarily small.

It is possible to make a rough estimate of the contribution given by a complex process using the formulae of direct processes with the heteroclinic area given by the unity (the area of the full phase space). Hence, ratios between the contributions for complex and direct processes are

$$\sqrt{A}\exp\left[-\frac{(1-A^{1/4})|\ln\hbar|}{S^{1/4}\pi}\right] \qquad \text{and} \qquad \sqrt{A}\exp\left[-\frac{(1-A^{1/4})}{S^{1/4}}\right]$$

for overlaps and Hamiltonian matrix elements, respectively. Therefore, for overlaps the ratio always goes to zero in the semiclassical limit. Moreover, for Hamiltonian matrix elements the ratio also goes to zero in practically all the cases because the homoclinic area being proportional to the inverse of the period results $S \sim 1/|\ln\hbar|$.[29]

In conclusion, the interaction between POs is dominated by a finite number of heteroclinic orbits; those describing a direct transition from one PO to the other. These heteroclinic orbits, grouped in pairs, define direct interaction schemes like that of figure 3. Each pair specifies an heteroclinic area, and only those areas smaller than S will be relevant for computing matrix elements.

Appendix E

In this appendix, we develop in detail the mathematical steps for going from equation (40) to equation (42). The calculation being trivial for $t_0(q) \equiv \frac{1}{2}\ln(2q^2/\hbar) = 0$, we assume that $t_0(q)/T$ tends to zero with $\hbar$ in order to replace the limits of integration in equation (40) by $\pm\infty$. Of course, this assumption limits the range of q where the calculation can be accomplished.

With the change of variable $z \equiv y - (T - 2t_0)$ (in the following we omit the argument of t_0), the error of the integral in equation (40) for modifying the upper limit becomes

$$A \equiv \left|\int_{T-2t_0}^{\infty} \cos\left[\frac{\pi}{2T}(y+2t_0)\right] \mathrm{e}^{-(\mathrm{e}^{-y}+y)/4}\,\mathrm{d}y\right| < \int_0^{\infty} \left|\cos\left(\frac{\pi}{2}+\frac{\pi z}{2T}\right)\right| \mathrm{e}^{-(z+T-2t_0)/4}\,\mathrm{d}z.$$

Moreover, as the effective integration range of the variable z is finite, we have $|\cos(\pi/2 + \pi z/2T)| \simeq \pi z/2T$. So, A is bounded by the relation

$$A < \frac{\pi\,\mathrm{e}^{-(T-2t_0)/4}}{2T}\int_0^{\infty} z\,\mathrm{e}^{-z/4}\,\mathrm{d}z \sim \frac{\mathrm{e}^{-(T-2t_0)/4}}{T}. \tag{E.1}$$

In the same way, with the change of variable $z \equiv -(y + T + 2t_0)$, the modulus of the lower part of the integral in the range $-\infty < y < -T - 2t_0$ becomes

$$B = \int_0^{\infty} \left|\cos\left(\frac{\pi}{2}+\frac{\pi z}{2T}\right)\right| \exp\left(\frac{-\mathrm{e}^{z+T+2t_0}+z+T+2t_0}{4}\right)\mathrm{d}z. \tag{E.2}$$

By expanding the exponent of the previous exponential function around $z = 0$

$$-\mathrm{e}^{z+\alpha}+z+\alpha = -\mathrm{e}^{\alpha}+\alpha-(\mathrm{e}^{\alpha}-1)z-|O(z^2)|$$

[29] Take into account that in a basis of scar functions the period of practically all the short periodic orbits is $\sim|\ln\hbar|$.

where $\alpha \equiv T + 2t_0$, we note that the effective range of integration in (E.2) goes to zero with $\hbar$. Hence, B is bounded by

$$B < \frac{\pi}{2T} \exp\left(\frac{-e^{\alpha} + \alpha}{4}\right) \int_0^{\infty} z \exp\left[-\left(\frac{e^{\alpha} - 1}{4}\right) z\right] dz < O\left[\frac{1}{T} \exp\left(-\frac{e^{T+2t_0}}{4}\right)\right]. \quad \text{(E.3)}$$

Consequently, by accepting an error $O(T^{-2})$ for the integral in (40), the limits of integration can be taken $\pm\infty$ if $A < O(T^{-2})$ and $B < O(T^{-2})$; moreover using equations (E.1) and (E.3), these conditions limit the range of validity to $q < O(T^{-2})$ and $q > \hbar\sqrt{2 \ln T}$, respectively.

Finally, by setting the limits $\pm\infty$ in equation (40), it is easy to derive (42); only note that

$$\int_{-\infty}^{\infty} \exp[-(e^{-y} + y)/4)] dy = \sqrt{2}\tilde{\Gamma}(1/4).$$

References

[1] Gutzwiller M C 1990 *Chaos in Classical and Quantum Mechanics* (New York: Springer)
[2] Voros A 1988 *J. Phys. A: Math. Gen.* **21** 685
[3] Berry M V and Keating J P 1990 *J. Physique* **23** 4839
Berry M V and Keating J P 1992 *Proc. R. Soc.* A **437** 151
[4] Vergini E G 2000 *J. Phys. A: Math. Gen.* **33** 4709
[5] Vergini E G and Carlo G G 2000 *J. Phys. A: Math. Gen.* **33** 4717
[6] Vergini E G and Carlo G G 2001 *J. Phys. A: Math. Gen.* **34** 4525
[7] Carlo G, Vergini E and Lustemberg P 2002 *J. Phys. A: Math. Gen.* **35** 7965
[8] Perelomov A 1986 *Generalized Coherent States and Their Applications* (Berlin: Springer)
[9] Courant R and Hilbert D 1966 *Methods of Mathematical Physics* (New York: Interscience)
[10] Lee S and Creagh S C 2003 *Ann. Phys.* **307** 392
[11] de Polavieja G G, Borondo F and Benito R 1994 *Phys. Rev. Lett.* **73** 1613
Kaplan L and Heller E J 1999 *Phys. Rev.* E **59** 6609
Wisniacki D, Borondo F, Vergini E and Benito R M 2001 *Phys. Rev.* E **63** 066220
Faure F, Nonnenmacher S and De Bievre S 2003 *Commun. Math. Phys.* **239** 449
[12] Littlejohn R G 1986 *Phys. Rep.* **138** 193
[13] Vergini E G 2004 *J. Phys. A: Math. Gen.* **37** 6507
[14] Wisniacki D, Vergini E, Benito R M and Borondo F 2004 *Phys. Rev.* E **70** 035202(R)
[15] Littlejohn R B 1990 *J. Math. Phys.* **31** 2952